Singlets in gauge theories with fundamental matter

Ed Bennett,[1,*] Ho Hsiao,[2,†] Jong-Wan Lee,[3,4,5,‡] Biagio Lucini,[1,6,§] Axel Maas,[7,∥]
Maurizio Piai,[8,¶] and Fabian Zierler[7,**]

[1]*Swansea Academy of Advanced Computing, Swansea University (Bay Campus), Fabian Way, SA1 8EN Swansea, Wales, United Kingdom*
[2]*Institute of Physics, National Yang Ming Chiao Tung University, 1001 Ta-Hsueh Road, Hsinchu 30010, Taiwan*
[3]*Particle Theory and Cosmology Group, Center for Theoretical Physics of the Universe, Institute for Basic Science (IBS), Daejeon 34126, Korea*
[4]*Department of Physics, Pusan National University, Busan 46241, Korea*
[5]*Institute for Extreme Physics, Pusan National University, Busan 46241, Korea*
[6]*Department of Mathematics, Faculty of Science and Engineering, Swansea University (Bay Campus), Fabian Way, SA1 8EN Swansea, Wales, United Kingdom*
[7]*Institute of Physics, NAWI Graz, University of Graz, Universitätsplatz 5, A-8010 Graz, Austria*
[8]*Department of Physics, Faculty of Science and Engineering, Swansea University (Park Campus), Singleton Park, SA2 8PP Swansea, Wales, United Kingdom*

(Received 24 July 2023; accepted 28 November 2023; published 5 February 2024)

We provide the first determination of the mass of the lightest flavor-singlet pseudoscalar and scalar bound states (mesons) in the Sp(4) Yang-Mills theory coupled to two flavors of fundamental fermions, using lattice methods. This theory has applications both to composite Higgs and strongly interacting dark matter scenarios. We find the singlets to have masses comparable to those of the light flavored states, which might have important implications for phenomenological models. We focus on regions of parameter space corresponding to a moderately heavy mass regime for the fermions. We compare the spectra we computed to existing and new results for SU(2) and SU(3) theories, uncovering an intriguing degree of commonality. As a by-product, in order to perform the aforementioned measurements, we implemented and tested, in the context of symplectic lattice gauge theories, several strategies for the treatment of disconnected-diagram contributions to two-point correlation functions. These technical advances set the stage for future studies of the singlet sector in broader portions of parameter space of this and other lattice theories with a symplectic gauge group.

DOI: 10.1103/PhysRevD.109.034504

I. INTRODUCTION

The possible existence of new strongly interacting sectors that extend the standard model (SM) of particle physics has been the subject of a long-standing history of theoretical studies. In recent years, this idea has been prominently featured in the context of composite Higgs models (CHMs) in which the Higgs fields of the SM originate as pseudo-Nambu-Goldstone bosons (PNGBs) of the underlying theory [1–3].[1] A parallel development has led to strongly coupled gauge theories being considered as the dynamical origin of hidden sectors in which dark matter consists of strongly interacting massive particles (SIMPs) [64–73]. This scenario can address observational problems, such as the *"core vs cusp"* [74] and *"too big to fail"* [75] ones, and have implications for gravitational wave experiments [76–93]—see, e.g., Refs. [94–99], as well as Refs. [100–104]. Both CHMs and SIMPs give rise to particles, the PNGBs, carrying nontrivial quantum numbers of non-Abelian global (flavor) symmetries, that suppress and protect their masses.

In general, strongly coupled theories also yield bound states that are flavor singlets. Composite models with a

*e.j.bennett@swansea.ac.uk
†thepaulxiao.sc06@nycu.edu.tw
‡j.w.lee@ibs.re.kr
§b.lucini@swansea.ac.uk
∥axel.maas@uni-graz.at
¶m.piai@swansea.ac.uk
**fabian.zierler@uni-graz.at

[1]The recent literature is vast. See, e.g., the reviews in Refs. [4–6], the summary tables in Refs. [7–9], and the selection of papers in Refs. [10–48] and Refs. [49–63].

strongly coupled origin can in particular give rise to a light dilaton [105–107], the PNGB associated with (approximate) scale invariance. The striking phenomenological implications of this possibility [108] have also been studied extensively (see, e.g., Refs. [109–120]), and the low energy effective field theory (EFT) of the dilaton [121,122] and the other PNGBs can be combined in the dilaton EFT [123–138]. Numerical evidence supporting this possibility has emerged in the context of SU(3) lattice gauge theories with special field content [139–151]. The singlet sector of a strongly coupled theory contains also pseudoscalar composite states, the phenomenology of which is the subject of dedicated studies [9,23,27,152–154]. Their EFT treatment follows closely that of axionlike particles (ALPs) [155–157].

The phenomenological consequences of such theories depend crucially on the mass spectrum of the lightest states and on the (model dependent) couplings to the standard model. While an efficient tool in treating the latter is provided by the EFT methodology, even the construction of such EFTs requires a good understanding of the lightest portion of the spectrum. Whatever the original motivation and application envisioned for such new strongly coupled physical sectors is, they have a plethora of bound states, some of which can be either stable or long lived, and potentially light. It is then desirable to gain a broad nonperturbative understanding of their spectroscopy, for all bound states, and in the largest possible portions of the parameter space. The instrument of choice for this endeavor is that of (numerical) lattice gauge theories. There has been a wide variety of investigations into the spectrum of many such theories, especially those with $\mathrm{SU}(N)$ group, with matter in various numbers and representations. Besides the aforementioned work, and Refs. [143,144,158–162] on SU(3), see, e.g., Refs. [163–171] for SU(2) theories, Refs. [172–175] for SU(4) in multiple representations, and [176] for G_2, as well as the reviews in Refs. [177–180].

Gauge theories with a symplectic group play a special role in all these contexts, because of the peculiar properties of $\mathrm{Sp}(2N)$ groups and their representations. For example, the model in Ref. [16] provides the simplest realization of a CHM that combines it with top partial compositeness [181] and consists of a $\mathrm{Sp}(2N)$ gauge theory with mixed-representation fermion content. Likewise, Refs. [64,66] use it for the construction of a SIMP-“miracle”. A number of recent lattice studies started to characterize them [182–198], following the pioneering effort in Ref. [199]. While much such work has focused on the spectroscopy of bound states carrying flavor, with this paper, we report on progress in the singlet sector.

The present study explores the flavor-singlet bound state sector in the Sp(4) gauge theory coupled to two fermions in the fundamental representation, a theory that has gathered substantial interest in the CHM context and also provides a minimal realization of the SIMP mechanism [67,69,71,72,200]. This study is complementary to the available nonsinglet hadron spectrum found in Refs. [182,184–187,189,190,197]. Within the general aim of understanding universal features of the low-lying spectrum across different gauge groups, this is also a step toward understanding how the approach to the large-N limit of $\mathrm{Sp}(2N)$ gauge theories differs from that of $\mathrm{SU}(N)$ gauge theories, especially with respect to the axial anomaly and topology. Our results could in the future help to understand the anomaly-mediated decays of singlets into SM particles.

We supplement this publication with numerical results obtained in two other theories. The first is the closely related SU(2) theory with two fundamental fermions, for which earlier studies exist [163,201], and for which we perform additional, new calculations. In the case of the SU(3) theory coupled to fermions in the fundamental representation, the pseudoscalar singlet has been studied in Refs. [202–214]. The determination of the mass (and width) of the lightest scalar singlet has proven to be particularly challenging, and a number of studies in SU(3) with dynamical fermions exists both in the context of real-world QCD [215–224] and more general field content [141,143,144,158–161]. We borrow results from this extensive literature for the purpose of comparing with our own results.

The paper is organized as follows. The pseudo-real nature of the fundamental representation of Sp(4)—as for SU(2)—leads to symmetry enhancement by modifying the flavor symmetry and symmetry-breaking pattern. The structure of the low-lying spectrum is hence different from the more familiar QCD case. We briefly comment on the most striking such features in Sec. II, as we define the continuum theory of interest. In Sec. III, we describe the lattice methods that we use to study the flavor-singlet states, putting some emphasis on the implications for the construction of suitable operators, in Sec. III A. The study of correlations functions involving singlets is affected by notorious difficulties, poor signal-to-noise ratio featuring prominently among them. This required the adoption of advanced techniques to obtain a nonzero signal, as we explain in Sec. III B, and in more detail in the Appendices.

We present the body of our numerical results in Sec. IV. Section IV A is devoted to the lightest pseudoscalar singlet state, in both the Sp(4) and SU(2) theories, for degenerate masses. We report on the case of nondegenerate flavor masses for Sp(4) (which realizes a scenario relevant to dark matter models) in Sec. IV B. The scalar singlet sector, in the degenerate case for the Sp(4) theory, is the subject of Sec. IV C, though we anticipate that, because of the bad signal-to-noise ratio, only a rough estimate with unclear finite-spacing systematics can be established at this stage. Finally, we assess our results by a comparison to the SU(3) case and report the results in Sec. IV D. Our general conclusion, exposed more critically in Sec. V, is that for the available range of fermion masses the singlets are indeed light enough to affect phenomenology and low-energy EFT considerations. We add several technical appendices, covering further details. We note that some preliminary results are available in Ref. [225].

II. FLAVOR SINGLETS IN SYMPLECTIC GAUGE THEORIES

We start the presentation by defining explicitly the (continuum) field theories of interest. We provide both their microscopic definition, in terms of elementary fields, and their salient long-distance properties, which can be explained in EFT terms. In doing so, we emphasize the role of the symmetries of the theory.

A. Microscopic theory and global symmetries

The $\mathrm{Sp}(2N)$ gauge theories of interest are characterized by a Lagrangian density, $\mathcal{L}$, which in this section, we write using a metric with Lorentzian signature $(+1,-1,-1,-1)$, and takes the form:

$$\mathcal{L} = -\frac{1}{2}\,\mathrm{Tr}[G_{\mu\nu}G^{\mu\nu}] + \bar{u}(i\gamma^{\mu}D_{\mu} - m_u)u + \bar{d}(i\gamma^{\mu}D_{\mu} - m_d)d, \tag{1}$$

where $G_{\mu\nu} \equiv \sum_A G^A_{\mu\nu}t^A$ are the field strength tensors, and t^A are the generators of $\mathrm{Sp}(2N)$, normalized so that $\mathrm{Tr}T^AT^B = \frac{1}{2}\delta^{AB}$, while u and d are four-component Dirac spinors, denoting the two flavors of fermion fields transforming in the fundamental representation of $\mathrm{Sp}(2N)$. The Lagrangian is real and Lorentz invariant, as $\bar{u} \equiv u^{\dagger}\gamma^0$, and $\bar{d} \equiv d^{\dagger}\gamma^0$. The covariant derivatives are defined in terms of the gauge fields $A_{\mu} \equiv A^A_{\mu}t^A$ as

$$D_{\mu}u \equiv \partial_{\mu}u + igA_{\mu}u, \qquad D_{\mu}d \equiv \partial_{\mu}d + igA_{\mu}d, \tag{2}$$

where g is the gauge coupling. Explicitly, the field-strength tensor is given by

$$G_{\mu\nu} \equiv \partial_{\mu}A_{\nu} - \partial_{\nu}A_{\mu} + ig[A_{\mu}, A_{\nu}], \tag{3}$$

where $[\cdot,\cdot]$ denotes the commutator.

The fundamental representation of $\mathrm{Sp}(2N)$ is pseudo-real. As a result, the global symmetry is enhanced: One can show explicitly, by rewriting Eq. (1) in terms of two-component fermions,[2] that for each Dirac fermion, the $\mathrm{U}(1)_L \times \mathrm{U}(1)_R$ Abelian global symmetry acting on its chiral projections is enhanced to a non-Abelian U(2) global symmetry. The fermion kinetic terms hence, written in terms of covariant derivatives, exhibit an enhanced (classical) $\mathrm{U}(4) = U(1)_A \times SU(4)$ global symmetry; we will return to the effect of anomalies in the next subsection.

The fermion mass terms break explicitly the global symmetry. If the masses are degenerate, $m_u = m_d$, as will be the case throughout most of this paper, then the global symmetry is explicitly broken to Sp(4). The bilinear, nonderivative operator appearing in the Lagrangian density as a mass term is also expected to condense so that the same symmetry breaking pattern appears also in spontaneous symmetry breaking effects. For generic choices of fermion masses, $m_u \neq m_d$, the approximate global symmetry is further broken to $\mathrm{Sp}(2)^2 \sim \mathrm{SU}(2)^2$ [197].

B. Light meson spectrum for two fundamental fermions

We summarize here the main properties of the bound states of interest, guided by gauge invariance and symmetry arguments, starting from the case in which the fundamental fermions have degenerate mass, $m_u = m_d$. We observe that the group structure has an even number of colors; hence baryons are bosons. Furthermore, because the matter content consists only of fermions transforming in the pseudo-real fundamental representation, and as a result, the global symmetry is enhanced, ordinary baryon number is a subgroup of the enhanced SU(4) and is unbroken in the vacuum of the theory, and hence objects that one might be tempted to classify as having different baryon number (e.g., mesons and diquarks) belong to the same Sp(4) multiplet.

We restrict the discussion from here onward to mesons made of two fundamental fermions. It may be convenient to think of the mesons in terms of their two-component fermion field content in order to classify them by their Sp(4) transformations and attribute their J^P quantum numbers.[3] As the two-component fermions transform as a 4 of Sp(4), the multiplication properties imply that there exist mesons transforming as a 1, 5, and 10 of Sp(4).

Starting from the spin-0 states, one expects to find in the spectrum 5 PNGBs, spanning the $\mathrm{SU}(4)/\mathrm{Sp}(4)$ coset, and transforming as a 5 of Sp(4), to become massless in the $m_u = m_d \to 0$ limit.[4] These states have parity partners, generalizing what in QCD literature are usually denoted as a_0 particles. Some numerical lattice evidence exists that at high

[2]This somewhat tedious exercise can be found in all its details in the literature, for instance, in Refs. [168,185] and references therein.

[3]We define the parity P so that flavor eigenstates are also parity eigenstates. See Refs. [165,185,197] for extended discussions of the subtleties involving twisting between space and flavor in the definition of parity.

[4]These are the states playing a role in CHMs; in their EFT description in terms of weakly coupled fields, four of them are identified with the components of the SM Higgs doublet because the $\mathrm{SU}(2)_L \times \mathrm{SU}(2)_R$ approximate symmetry of the electroweak theory is identified with the $SO(4)$ subgroup of Sp(4), and hence $5 = 4 \oplus 1$ [16]. The 1 is an additional state that carries no SM gauge quantum numbers, but in the EFT description of the strong coupling sector, it is degenerate with the 4. Likewise, these states are the dark matter candidates in SIMP models [64,65,197].

temperature, these two sets of states become degenerate—see Ref. [226] for SU(2) and Ref. [227] for SU(3), both with two flavors of fundamental fermions—because the $\mathrm{U}(1)_A$ symmetry relating them is restored, but at zero temperature the scalar 5 is expected to be heavy, the mass of the particles being of the order of the confinement scale, even in the $m_u = m_d \to 0$ limit.

Classically, one would expect also two singlet scalars to be light: the axion and the dilaton. Indeed, the classical Lagrangian for $m_u = m_d = 0$ is invariant also under the action of a $\mathrm{U}(1)_A$ symmetry and of dilatations, the condensates breaking both of them spontaneously, and these two additional light states can be thought of as the PNGBs associated with these two Abelian symmetries. Alas, besides being explicitly broken by the fermion masses, both these symmetries are also anomalous. The $\mathrm{U}(1)_A$ and scale anomalies hence provide masses for the axion-dilaton system, related to the scale of confinement of the theory. Mixing effects between these states and other vacuum excitations (e.g., glueballs with the same J^P quantum numbers) are present as well, given that no symmetry argument can be invoked rigorously to forbid them. The precise determination of such masses, hence, is nontrivial, and to large extent this paper is about setting the stage for its future large-scale, high-precision calculation. Furthermore, in confining theories with large numbers of degrees of freedom, and when approaching the lower edge of the conformal window, nonperturbative effects might suppress the mass of the axion and dilaton, respectively; this is a very active field of research in itself, for a potential phenomenological role both of this axion and of the dilaton, as we mentioned in the introduction; the technology we developed and tested for this paper could play an important future role in either case.

The spin-1 part of the meson spectrum is more rich. In analogy with the case of QCD, one expects the lightest of such states to generalize the ρ mesons; they transform as a 10 of Sp(4) and have $J^P = 1^-$, and their properties have been studied elsewhere [184]. They have the peculiar property that they can be sourced by two different interpolating operators, with the schematic structures $\bar{\psi}\gamma_\mu\psi$ and $\bar{\psi}\sigma_{\mu\nu}\psi$, respectively. In addition, the generalizations of the a_1 and b_1 from QCD transform as a 5 and a 10 of Sp(4), respectively; these additional states are heavier than the aforementioned 10-plet with $J^P = 1^-$—see the discussions in Refs. [168,185]. It is worth noticing that some spin-1 singlet mesons of QCD are actually part of these multiplets because of the symmetry-enhancement pattern—noticeably, the particle that corresponds to ω in QCD.

In the presence of nondegenerate fermion masses, $m_u \neq m_d$, the global symmetry breaks further from Sp(4) down to $\mathrm{Sp}(2) \times \mathrm{Sp}(2) = \mathrm{SU}(2) \times \mathrm{SU}(2) \sim \mathrm{SO}(4)$. Consequently, the multiplets decompose with respect to the smaller flavor symmetry [197]. The 5-plets split into a 4-plet and a singlet, whereas the 10-plet decomposes into a 6-plet and a 4-plet. This implies that an additional singlet appears in states that would have been a 5-plet in the mass-degenerate theory, such as the PNGBs and the axial vectors. This is the familiar scenario in QCD: In the presence of a mass difference between up and down quark, isospin is explicitly broken, and the flavor-neutral pion π^0 becomes a singlet, with different mass from the charged $\pi^\pm$ states. The main difference with QCD is that, as the pseudo-reality of the representation results in additional flavor neutral states, which microscopically can be written as di-quark states, the multiplet is enlarged.

This differs for mesons in the 10-plet representation, such as the vector meson. The 10 decomposes in a 4-plet (with the same flavor structure as in the case of the PNGBs) and a 6-plet. The latter consists of two states sourced by ordinary meson operators (in the QCD analogy, they are the ρ^0 and the ω particles with $J^P = 1^-$) and four other states that are sourced by diquark operators. A further splitting of these multiplets is possible, for example, by gauging a U(1) subgroup of the SO(4) symmetry [197], but we do not consider it here.

III. LATTICE SETUP

We perform lattice simulations using the standard plaquette action and standard Wilson fermions [228]. We use the HiRep code [229,230] extended for $\mathrm{Sp}(2N)$ gauge theories [231] to generate configurations and to perform the measurements. In the case of degenerate fermions, we use the hybrid Monte Carlo (HMC) [232] algorithm, and for nondegenerate fermions, we use the rational HMC (RHMC) [233] algorithm. The latter case does not guarantee positivity of the fermion determinant. In this case, we have monitored the lowest eigenvalue of the Dirac operator, which we always found to be positive. Thus, we do not see any hints of a sign problem for the fermion masses studied in this work. Results for the nonsinglet spectrum for two fundamental fermions were first reported in Refs. [185,197]. We give simulation details of our ensembles in Tables I and II.

We perform simulations on Euclidean lattices of size $T \times L^3$ and define the bare inverse gauge coupling as $\beta = 8/g^2$. We implement periodic boundary conditions for the gauge fields. For the Dirac fields, we impose periodic boundary conditions in the spatial directions and antiperiodic boundary conditions in the temporal direction.

A. Interpolating operators and two-point functions

We use fermion bilinear operators for sourcing both singlet and nonsinglet mesons. From here onward, with some abuse of notation, we denote as η' and σ, respectively, the pseudoscalar and scalar, flavor-singlet states. While the mesonic sectors are enlarged in $\mathrm{Sp}(2N)$ with fundamental fermions, every nonsinglet or singlet state can still be

TABLE I. List of all ensembles with degenerate fermion masses used in this work. We report the number of configurations n_{conf}, the number of the stochastic sources used in the approximation of the all-to-all quark propagator n_{src}, the intervals for fitting the resulting meson correlators I_{meson}, and the average value of the plaquette $\langle P \rangle$. In some cases, we were unable to identify a clear plateau in the effective masses and could not determine the singlet masses. In these cases, we do not report a fit interval. For the singlet mesons, the interval quoted here was used to fit the correlators after subtracting the excited state contributions in the connected pieces and after performing a numerical derivative.

Ensemble	Group	β	m_0	L	T	n_{conf}	n_{src}	$I_{\eta'}$	I_π	I_σ	$I_{\sigma^{\mathrm{conn}}}$	I_ρ	$\langle P \rangle$
SU2B1L1M8	SU(2)	2.0	−0.947	20	32	1020	300	⋯	(10, 16)	(5, 8)	(7, 10)	(10, 16)	0.56734(2)
SU2B1L1M7	SU(2)	2.0	−0.94	14	24	1851	192	(8, 12)	(8, 12)	⋯	⋯	(9, 12)	0.56516(3)
SU2B1L1M6	SU(2)	2.0	−0.935	16	32	951	256	(7, 11)	(9, 16)	⋯	⋯	(9, 16)	0.563654(28)
SU2B1L1M5	SU(2)	2.0	−0.93	14	24	1481	256	(7, 12)	(8, 12)	⋯	⋯	(9, 12)	0.56245(3)
SU2B1L1M4	SU(2)	2.0	−0.925	14	24	1206	192	(6, 10)	(8, 12)	⋯	⋯	(9, 12)	0.56119(3)
SU2B1L1M3	SU(2)	2.0	−0.92	12	24	2401	192	(6, 9)	(7, 12)	⋯	(6, 11)	(8, 12)	0.559983(29)
SU2B1L1M2	SU(2)	2.0	−0.9	12	24	500	128	(6, 9)	(7, 12)	⋯	⋯	(8, 12)	0.55571(6)
SU2B1L1M1	SU(2)	2.0	−0.88	10	20	2582	128	(5, 8)	(8, 10)	⋯	⋯	(9, 10)	0.55225(4)
Sp4B3L1M8	Sp(4)	7.2	−0.799	32	40	451	224	⋯	(15, 20)	(5, 9)	(11, 19)	(15, 20)	0.590862(5)
Sp4B3L1M7	Sp(4)	7.2	−0.794	28	36	504	288	(7, 12)	(10, 18)	⋯	(11, 16)	(11, 18)	0.590452(7)
Sp4B3L1M6	Sp(4)	7.2	−0.79	24	36	500	320	(7, 12)	(12, 18)	(5, 8)	(10, 16)	(13, 18)	0.590127(9)
Sp4B3L1M5	Sp(4)	7.2	−0.78	24	36	508	384	(6, 12)	(12, 18)	⋯	(11, 15)	(13, 18)	0.589278(8)
Sp4B3L1M4	Sp(4)	7.2	−0.77	24	36	200	384	(6, 11)	(11, 18)	⋯	(10, 15)	(12, 18)	0.588460(12)
Sp4B3L1M3	Sp(4)	7.2	−0.76	16	36	200	384	⋯	(11, 18)	(5, 8)	(9, 14)	(12, 18)	0.587666(25)
Sp4B1L1M7	Sp(4)	6.9	−0.924	24	32	492	320	⋯	(9, 16)	(4, 7)	(7, 10)	(10, 16)	0.56317(2)
Sp4B1L1M6	Sp(4)	6.9	−0.92	24	32	503	484	⋯	(7, 16)	(4, 9)	(8, 12)	(8, 16)	0.562075(13)
Sp4B1L2M6	Sp(4)	6.9	−0.92	16	32	176	128	(6, 10)	(9, 16)	(4, 10)	(7, 10)	(9, 16)	0.56212(5)
Sp4B1L1M5	Sp(4)	6.9	−0.91	16	32	435	256	(6, 11)	(8, 16)	⋯	(7, 9)	(9, 16)	0.55935(3)
Sp4B1L2M5	Sp(4)	6.9	−0.91	14	24	513	256	(5, 10)	(8, 12)	(4, 7)	(9, 12)	(9, 12)	0.55941(3)
Sp4B1L1M4	Sp(4)	6.9	−0.9	16	32	547	512	(6, 10)	(9, 16)	⋯	(7, 10)	(10, 16)	0.556921(25)
Sp4B1L2M4	Sp(4)	6.9	−0.9	14	24	942	128	(7, 10)	(8, 12)	(4, 9)	(7, 9)	(9, 12)	0.556981(26)
Sp4B1L3M4	Sp(4)	6.9	−0.9	12	24	2904	128	(6, 10)	(8, 12)	(4, 8)	(8, 10)	(9, 12)	0.557009(18)
Sp4B1L2M3	Sp(4)	6.9	−0.89	14	24	461	128	(7, 10)	(8, 12)	(5, 9)	(8, 11)	(9, 12)	0.55468(4)
Sp4B1L3M3	Sp(4)	6.9	−0.89	12	24	1019	320	(6, 10)	(8, 12)	(3, 6)	(7, 11)	(9, 12)	0.55467(3)
Sp4B1L2M2	Sp(4)	6.9	−0.87	12	24	1457	128	(7, 11)	(8, 12)	(5, 8)	(8, 10)	(9, 12)	0.550497(27)
Sp4B1L2M3	Sp(4)	6.9	−0.87	10	20	976	128	(6, 9)	(8, 10)	⋯	(6, 10)	(8, 10)	0.55068(5)

probed by fermion-antifermion operators, even in the case of nondegenerate fermions. Furthermore, since fermions are moderately heavy, we find such operators are sufficient to study the ground states and for now do not consider others (such as $\pi\pi$ operators, glueballs, or even tetraquarks). We use the operators

$$O_1^{(\Gamma)}(n) = \bar{u}(n)\Gamma d(n),$$
$$O_\pm^{(\Gamma)}(n) = (\bar{u}(n)\Gamma u(n) \pm \bar{d}(n)\Gamma d(n))/\sqrt{2}, \qquad (4)$$

where $n = (\vec{n}, t)$ denote lattice sites. For pseudoscalar mesons, $\Gamma = \gamma_5$, and we omit the superscript when its

TABLE II. List of all ensembles with nondegenerate fermion masses used in this work. We report the number of configurations n_{conf}, the number of the stochastic sources used in the approximation of the all-to-all quark propagator n_{src}, the intervals for fitting the resulting meson correlators I_{meson}, and the average value of the plaquette $\langle P \rangle$. In some cases, we were unable to identify a clear plateau in the effective masses and could not determine the singlet masses. In these cases, we do not report a fit interval. For the singlet mesons, the interval quoted here was used to fit the correlators after subtracting the excited state contributions in the connected pieces and after performing a numerical derivative.

Ensemble	β	m_0^1	m_0^2	L	T	n_{conf}	n_{src}	$I_{\eta'}$	I_{π^0}	$I_{\pi^\pm}$	I_σ	$I_{\sigma^{\mathrm{conn}}}$	I_ρ	$\langle P \rangle$
Sp4B1L2M4ND1	6.9	−0.9	−0.89	14	24	300	64	(7, 10)	(7, 10)	(8, 14)	(4, 8)	(8, 14)	(8, 14)	0.55583(5)
Sp4B1L2M4ND2	6.9	−0.9	−0.88	14	24	191	128	(7, 10)	(7, 10)	(8, 14)	(4, 8)	(8, 14)	(8, 14)	0.55474(5)
Sp4B1L2M4ND3	6.9	−0.9	−0.87	14	24	400	128	(7, 10)	(7, 10)	(8, 14)	(5, 8)	(8, 14)	(8, 14)	0.55361(4)
Sp4B1L2M4ND4	6.9	−0.9	−0.85	14	24	300	64	⋯	⋯	(8, 14)	(5, 8)	(8, 14)	(8, 14)	0.55163(4)
Sp4B1L2M4ND5	6.9	−0.9	−0.8	14	24	400	128	(7, 10)	(7, 10)	(8, 14)	⋯	(8, 14)	(8, 14)	0.54735(4)
Sp4B1L2M4ND6	6.9	−0.9	−0.75	12	24	264	64	(7, 10)	(7, 10)	(8, 12)	⋯	(8, 12)	(8, 12)	0.54395(6)
Sp4B1L2M4ND7	6.9	−0.9	−0.7	12	24	249	128	(7, 10)	(7, 10)	(8, 12)	⋯	(8, 12)	(8, 12)	0.54104(6)

value is clear from the context. The pseudoscalar operators O_- and O_1 source the pion 5-plet, and the operator O_+ sources the pseudoscalar singlet, η'. The same pattern persists for the scalar mesons where $\Gamma = 1$, and we use the notation:

$$O_{\eta'}(n) \equiv (\bar{u}(n)\gamma_5 u(n) + \bar{d}(n)\gamma_5 d(n))/\sqrt{2},$$
$$O_\sigma(n) \equiv (\bar{u}(n)u(n) + \bar{d}(n)d(n))/\sqrt{2}. \qquad (5)$$

For vector mesons, $\Gamma = \gamma_i$, and all operators O_1 and $O_\pm$ source states in the vector 10-plet [185]. In the nondegenerate case, the flavored multiplet is always probed by O_1. For the vector mesons, both O_- and O_+ probe the same unflavored multiplet. In the case of the pseudoscalars and scalars, the O_- and O_+ probe distinct singlets. We note that the ensembles studied in this work have moderately heavy fermions—in all cases, the vector meson is lighter than twice the pNGB mass. After performing the required Wick contractions, we arrive at the following two-point correlation functions:

$\langle O_1(n)\bar{O}_1(m)\rangle = -$ 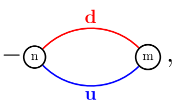 ,

$2\langle O_\pm(n)\bar{O}_\pm(m)\rangle = -$ 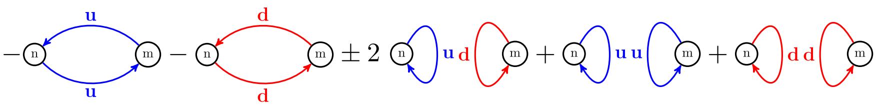 . (6)

It can be seen that the singlet mesons only differ from the nonsinglets by the additional disconnected diagrams. In the degenerate limit, they cancel exactly for the O_- operators. In order to determine the mesonic spectrum, we need to determine both the connected and disconnected pieces and then fit the zero momentum correlator,

$$C(t) \equiv \sum_{\vec{n}} \langle O(\vec{n}, t)\bar{O}(\vec{0}, 0)\rangle, \qquad (7)$$

on a Euclidean time interval $(t_{\text{min}}, t_{\text{max}})$, where the ground state dominates, and its energy—and thus the mass—can be extracted. The different components of $C(t)$ drop off exponentially with their energy $\propto \exp(-E_n t)$, and thus at sufficiently large t, only the ground state remains, as all other states are exponentially suppressed. However, we note that an additional constant term can arise, which is the case for both the η' and the σ meson. In the former case, this can arise due to an insufficient topological sampling of the path integral, and this constant vanishes in the continuum limit [234,235]. For the scalar singlet, σ, this constant arises due to the vacuum contributions, e.g., the fermion condensate, and persists in the continuum limit for vanishing momenta. At large times, the correlator $C(t)$ is then given by

$$\lim_{t\to\infty} C(t) = a(e^{-mt} + e^{-m(T-t)}) + \langle 0|O|0\rangle^2, \qquad (8)$$

where the second exponential term is due to the lattice periodicity. While in the case of the η', this constant is small compared to the signal and only affects the correlator at large t, this is not the case for the σ meson. In the scalar case, this constant is several orders of magnitudes larger than the signal, and its removal is a significant challenge.

We choose to perform a numerical derivative as proposed in Ref. [236]. The resulting correlator is then antisymmetric with respect to the midpoint $T/2$,

$$\tilde{C}(t) \equiv \frac{1}{2}(C(t-1) - C(t+1)) \overset{t\to\infty}{\longrightarrow} a \sinh(m) \times (e^{-mt} - e^{-m(T-t)})). \qquad (9)$$

In order to determine the Euclidean time interval for fitting, we use an effective mass $m_{\text{eff}}(t)$ defined by

$$\frac{\tilde{C}(t-1)}{\tilde{C}(t)} = \frac{e^{-m_{\text{eff}}(t)\cdot(T-t+1)} \pm e^{-m_{\text{eff}}(t)\cdot(t-1)}}{e^{-m_{\text{eff}}(t)\cdot(T-t)} \pm e^{-m_{\text{eff}}(t)\cdot t}}, \qquad (10)$$

where the $+$ is used for periodic correlators, and the $-$ sign in case of antiperiodic correlators with respect to the lattice midpoint $T/2$. We determine $(t_{\text{min}}, t_{\text{max}})$ by visually inspecting the effective mass and identifying a plateau at large times t. We restrict ourselves to ensembles where the plateau persists over four or more time slices. We then perform a fit of a single exponential term to the correlator $\tilde{C}(t)$ for the mesons. In Appendix A, we compare this method to computing the additional constant $\langle 0|O|0\rangle^2$ directly, without the use of a numerical derivative.

For the pseudoscalar sector in the nondegenerate $N_f = 1+1$ theory, both the π^0 and η' are pseudoscalar singlets, and the η' is not a ground state. Thus, we need to perform a variational analysis by computing the correlation matrix of the operators O_{π^0} and $O_{\eta'}$ and solve the resulting generalized eigenvalue problem (GEVP). In the minimal operator basis of (4) and (5), the cross-correlator are diagrammatically given by

$$2\langle O_+(n)\bar{O}_-(m)\rangle = - \quad (11)$$

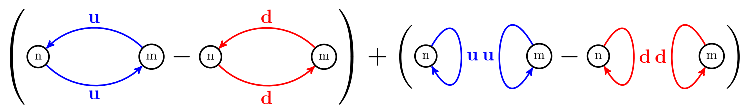

In the mass-degenerate limit, the cross-correlator vanishes, and the η' becomes the ground state of the pseudoscalar singlet sector, whereas the π^0 becomes part of the pNGB multiplet. Note the presence of connected diagrams in the cross-correlator. This implies that even in the limit of large fermion masses—which suppresses the disconnected pieces—the cross-correlator remains large for large mass differences, i.e., a system with heavy-light properties. Thus, sizeable mixing effects are expected to occur.

For a heavy-light system, a more diagonal basis is obtained by using the operators $O_A^{\rm PS} = \bar{u}\gamma u$ and $O_B^{\rm PS} = \bar{d}\gamma d$. The corresponding cross-correlator vanishes as the heavier fermion mass approaches infinity and is given by

$$\langle O_A^{PS}(n)\bar{O}_B^{PS}(m)\rangle = \quad (12)$$

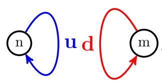

B. Variance reduction techniques

In order to obtain the full singlet two-point functions, we need to measure both the connected and disconnected pieces in Eq. (6). The disconnected diagrams in particular are very noisy, and the signal is already lost at small to intermediate t where contaminations from excited states are non-negligible. A direct determination of the ground state mass at large t is thus not possible. We can circumvent this problem by removing the contributions of excited states in the singlet correlators manually. This is straightforward for the connected pieces. There, the signal for the connected pseudoscalar and vector mesons persists for all time slices t, and in the case of the connected piece of the scalar meson, we still have a signal up to large t. We fit the connected piece at large times (see Tables I and II for our choice of fit intervals) to a single exponential

$$C_{\rm conn}^{1\,\rm exp}(t) = A_0(e^{-m_{\rm conn}t} + e^{-m_{\rm conn}(T-t)}), \quad (13)$$

and replace the full connected piece by the ground state correlator [237], where A_0 and $m_{\rm conn}$ are the fit parameters, such that

$$C_{\eta'}^{1\,\rm exp}(t) = C_{\pi,\rm conn}^{1\,\rm exp}(t) + C_{\eta',\rm disc}(t), \quad (14)$$

$$C_{\sigma}^{1\,\rm exp}(t) = C_{\sigma,\rm conn}^{1\,\rm exp}(t) + C_{\sigma,\rm disc}(t). \quad (15)$$

We find that the excited state contributions in the connected pieces are the dominant ones, and removing them shows a much earlier onset of a plateau in the effective masses. The underlying assumption for these correlators is that the excited state contributions of full and connected pieces are indistinguishable within data quality as was noted in [209]. This is not guaranteed *a priori*. However, we find that the excited state contributions in the connected pieces are indeed the dominant ones. In Appendix B, we show that our results obtained by subtracting the connected excited state contributions through a fit at larger times produces the same results as using smeared operators for the connected pieces with more overlap with the ground state.

Note that this technique is not applicable to the non-degenerate case, as the η' is no longer a ground state and some relevant information is actually encoded in the excited states. Thus, we will not apply this technique there.

The evaluation of disconnected pieces requires all-to-all propagators. We use $Z_2 \times Z_2$ noisy sources with spin and even-odd dilution [238]. We typically use $\mathcal{O}(100)$ distinct noise vectors. The connected pieces are evaluated using stochastic wall sources. Uncertainties are estimated using the jackknife method.

IV. RESULTS

Here we report the main results of our numerical investigations on the mass spectrum of flavor-singlet pseudoscalar and scalar mesons, obtained using the techniques discussed in the previous section. We focus on the Sp(4) theory coupled to two fundamental dynamical fermions, but for degenerate fermions, we supplement it with the SU(2) theory with the same matter content. In the case of the pseudoscalar singlet, we further compare to the existing literature on lattice results for the SU(3) theory.

A. Pseudoscalar singlet in SU(2) and Sp(4) with $N_f = 2$

Our results for the mesons with degenerate fermions are tabulated in Table III. All the ensembles satisfy the condition $m_\pi L > 6$, suggested by the observations in Ref. [184] for Sp(4), and in Ref. [166] for SU(2), that the size of finite volume corrections to the low-lying spectrum for flavored mesons is of the order of 1–2% at $m_\pi L \simeq 6$ and becomes much smaller for the larger volumes, as it is exponentially suppressed with the volume. This observation is also confirmed by our measurements of m_π and m_ρ at different volumes in the Sp(4) theory with $\beta = 6.9$ by varying the bare fermion mass, m_0. Finite volume corrections to $m_{\eta'}$ are compatible with the statistical uncertainties and expected to be less than 2%, which we estimated from the most precise results available, for

TABLE III. The light spectrum of SU(2) and Sp(4) with degenerate fermions: the lightest flavored pseudoscalar, π, and vector, ρ, and flavor-singlet pseudoscalar, η', and scalar, σ, mesons, measured in different ensembles. All dimensionful quantities are given in lattice units and the omission of the lattice spacing $a = 1$ is understood. The missing entries for $m_{\eta'}$ and/or m_σ are due to the measurements not fulfilling the fitting criteria discussed in the main text.

	β	m_0	L	T	$m_\pi L$	m_π/m_ρ	m_π	m_ρ	$m_{\eta'}$	m_σ
SU(2)	2.0	−0.947	20	32	7.47(3)	0.690(7)	0.3735(13)	0.540(5)	⋯	0.53(4)
SU(2)	2.0	−0.94	14	24	6.40(2)	0.746(6)	0.4576(14)	0.612(4)	0.67(6)	⋯
SU(2)	2.0	−0.935	16	32	7.91(2)	0.767(5)	0.4946(14)	0.644(4)	0.60(3)	⋯
SU(2)	2.0	−0.93	14	24	7.491(19)	0.787(4)	0.5350(14)	0.679(3)	0.65(3)	⋯
SU(2)	2.0	−0.925	14	24	7.999(19)	0.806(4)	0.5713(14)	0.708(3)	0.634(16)	⋯
SU(2)	2.0	−0.92	12	24	7.323(10)	0.8210(19)	0.6102(8)	0.7432(14)	0.665(9)	⋯
SU(2)	2.0	−0.9	12	24	8.620(17)	0.862(3)	0.7183(14)	0.832(2)	0.770(16)	⋯
SU(2)	2.0	−0.88	10	20	8.120(11)	0.885(2)	0.8120(11)	0.9169(19)	0.842(5)	⋯
Sp(4)	7.2	−0.799	32	40	8.087(16)	0.668(4)	0.2527(5)	0.377(2)	⋯	0.36(5)
Sp(4)	7.2	−0.794	28	36	8.072(11)	0.710(2)	0.2882(4)	0.4055(11)	0.397(16)	⋯
Sp(4)	7.2	−0.79	24	36	7.505(19)	0.742(6)	0.3127(8)	0.421(3)	0.387(13)	0.56(6)
Sp(4)	7.2	−0.78	24	36	8.882(17)	0.793(4)	0.3700(7)	0.466(2)	0.418(7)	⋯
Sp(4)	7.2	−0.77	24	36	10.16(2)	0.829(5)	0.4236(10)	0.510(3)	0.456(8)	⋯
Sp(4)	7.2	−0.76	16	36	7.544(17)	0.850(4)	0.4715(10)	0.554(2)	⋯	0.64(12)
Sp(4)	6.9	−0.924	24	32	8.208(12)	0.663(2)	0.3420(5)	0.5157(17)	⋯	0.46(3)
Sp(4)	6.9	−0.92	24	32	9.356(12)	0.7036(17)	0.3898(5)	0.5540(12)	⋯	0.42(2)
Sp(4)	6.9	−0.92	16	32	6.22(2)	0.696(7)	0.3889(14)	0.558(5)	0.49(3)	0.45(6)
Sp(4)	6.9	−0.91	16	32	7.817(19)	0.769(5)	0.4885(12)	0.634(4)	0.560(14)	⋯
Sp(4)	6.9	−0.91	14	24	6.86(2)	0.766(6)	0.4902(16)	0.639(5)	0.541(9)	0.41(3)
Sp(4)	6.9	−0.9	16	32	9.006(13)	0.815(3)	0.5629(8)	0.690(2)	0.611(9)	⋯
Sp(4)	6.9	−0.9	14	24	7.897(14)	0.812(3)	0.5641(10)	0.694(2)	0.619(16)	0.57(4)
Sp(4)	6.9	−0.9	12	24	6.796(9)	0.809(2)	0.5663(8)	0.6994(18)	0.610(6)	0.55(2)
Sp(4)	6.9	−0.89	14	24	8.813(19)	0.843(4)	0.6295(13)	0.746(3)	0.69(2)	0.57(9)
Sp(4)	6.9	−0.89	12	24	7.581(15)	0.841(3)	0.6318(12)	0.751(3)	0.661(9)	0.62(7)
Sp(4)	6.9	−0.87	12	24	8.925(10)	0.878(2)	0.7437(9)	0.8468(17)	0.782(13)	0.80(15)
Sp(4)	6.9	−0.87	10	20	7.470(16)	0.871(3)	0.7470(16)	0.857(3)	0.764(9)	⋯

$m_0 = -0.9$, if $m_\pi L \gtrsim 6$. We therefore safely neglect finite volume corrections to $m_{\eta'}$ in the following.

In Fig. 1, we present our measurements of the ratios between the mass of the η' meson and that of the pseudoscalar nonsinglet π, as a function of m_π/m_ρ. For reference, we indicate the mass of the vector meson ρ by a solid line. In the Sp(4) theory, we find that the pseudoscalar singlet is consistently heavier than the nonsinglet, over the range of $0.7 \lesssim m_\pi/m_\rho \lesssim 0.9$, but lighter than the vector mesons. While in the lightest and finest ensembles, the hierarchy between the pseudoscalar singlet and vector mesons is not yet clearly resolved, the emerging trend is that $m_{\eta'}/m_\pi$ slowly increases as m_π decreases in this mass regime and approaches m_ρ/m_π for $m_\pi/m_\rho \lesssim 0.75$. We do not observe an appreciable difference in the mass ratios obtained with the two different values of β, within the quoted one-sigma error bars. We find a similar trend in the SU(2) theory, as shown in the right panel of Fig. 1. Since in this case only one fairly coarse lattice is considered, we cannot comment on the size of finite lattice spacing effects.

The smallness of lattice artifacts in the ratios of meson masses is somewhat surprising, as the lattice spacing for $\beta = 7.2$ is approximately 40% smaller than for $\beta = 6.9$ [184]. To assess this point, we present the meson masses in units of the gradient flow scale w_0, which defines a common scale in the continuum theory, and which we use also to compute the topological charge Q—see Appendix A. We borrow the definition and measurements of the gradient flow scale w_0 from Ref. [184] and refer the reader to that publication for details. The left panel of Fig. 2 shows that both the mass of the pseudoscalar singlet and the vector mesons receive significant corrections from the finite lattice spacing. By comparing with Fig. 1, we see that such corrections to $m_\pi w_0$ and $m_{\eta'} w_0$ happen to have the same sign and similar sizes, which cancel out in the mass ratios. We observe the same pattern for the mass ratio of m_ρ and $m_{\eta'}$, as depicted in the right panel of Fig. 2.

B. Pseudoscalar singlets in Sp(4) with $N_f = 1 + 1$

For nondegenerate fermions, the theory contains two flavor-singlet pseudoscalar mesons, the η' as well as the flavor-diagonal PNGB, π^0. To understand the effects of (explicit) flavor-symmetry breaking on the low-lying spectrum, we first choose the ensemble for degenerate fermions with $\beta = 6.9$ and $m_0 = -0.9$ and vary the bare mass of one of the Dirac fermion, $m_0^{(2)} \geq m_0$, for which we effectively increase its mass, while keeping that of the other fixed,

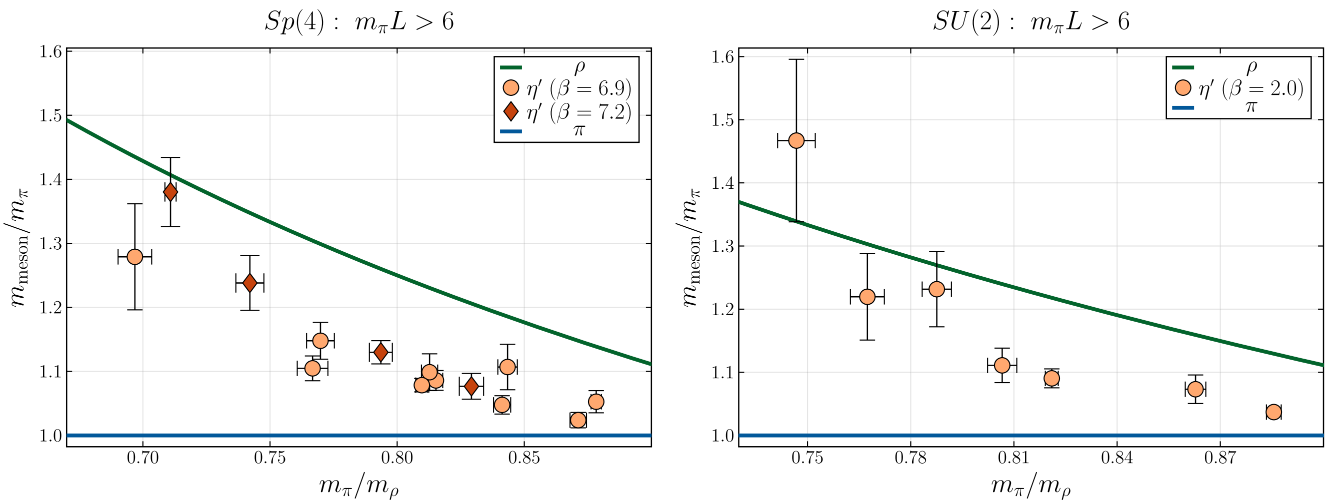

FIG. 1. Left panel: Mass ratios $m_{\rm meson}/m_\pi$ for pseudoscalar and vector mesons, including the flavor-singlet pseudoscalar η', in the Sp(4) gauge theory with $N_f = 2$ Dirac flavors of fermions in the fundamental representation measured at the two values of the inverse coupling $\beta = 6.9$ and 7.2. Right panel: The same plot but in the SU(2) gauge theory at $\beta = 2.0$. The green solid lines $m_\rho/m_\pi = 1/x$ are displayed for reference.

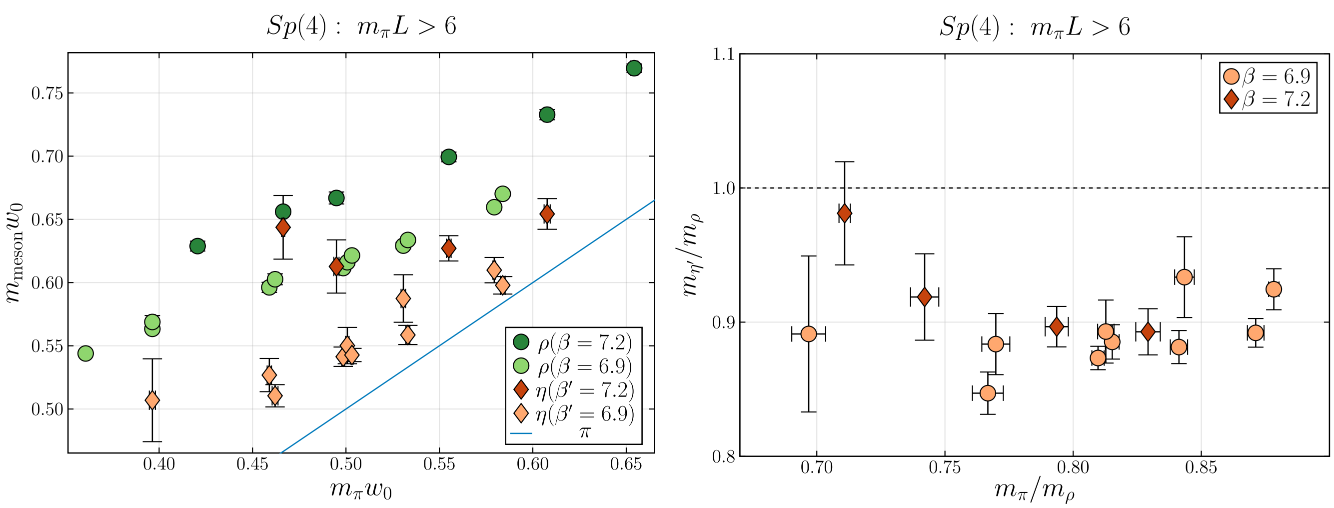

FIG. 2. Left panel: Same data as in the left panel of Fig. 1, but now masses are given in units of the gradient flow scale w_0. The blue solid line $w_0 m_\pi = x$ is displayed for reference. Right panel: Mass ratio between of the vector mesons ρ and the scalar singlet η'.

$m_0^{(1)} = m_0$. We summarize the numerical results in Table IV. In the table, we also present the mass of the flavor-singlet PNGB obtained by computing only the connected diagrams after dropping the last three terms in Eq. (6), which we denote by $m_{\pi_c^0}$. Within the generally larger uncertainties, we find no statistically appreciable difference between m_{π^0} and $m_{\pi_c^0}$, which supports the connected-only approximation considered in Ref. [197].

In the left panel of Fig. 3, we show the meson masses, as a function of the flavoured pNGBs mass $m_{\pi^\pm}$. In the mass-degenerate limit, we recover the mass hierarchy of Sec. IV A, as expected. As we increase one of the fermion masses, we observe a clear separation between flavored mesons and the unflavored π^0 as well as the unflavored vector mesons ρ^0, with the former being heavier than the latter. At the same time, the pseudoscalar singlet η', becomes heavier. This effect leads to an inversion of the mass hierarchy between the vector mesons $\rho^\pm$, ρ^0, and the η' meson, and the η' becomes heavier than any other meson considered here.[5]

A couple of cautionary remarks should be added. First of all, we are in a moderately heavy mass regime, with

[5]This is qualitatively different from the preliminary results in [225], where the mixing between the pseudoscalar singlets was neglected, and the excited state subtraction of Sec. III B was incorrectly applied to the nondegenerate theory.

TABLE IV. Results for the light spectrum with nondegenerate fermions: the flavored pseudoscalar $\pi^{\pm}$ and vector $\rho^{\pm}$, and the flavor-singlet pseudoscalar η', π^0, vector ρ^0 and scalar σ mesons. All dimensionful quantities are given in lattice units ($a = 1$). Missing entries for $m_{\eta'}$ or m_σ denote measurements that do not fulfill the fitting criteria discussed in the main text. We furthermore report the mass of the flavor-singlet pseudo-Goldstone $m_{\pi^0_c}$ in the connected-only approximation.

β	$m_0^{(1)}$	$m_0^{(2)}$	L	T	m_{π^0}	$m_{\pi^0_c}$	$m_{\pi^{\pm}}$	m_{ρ^0}	$m_{\rho^{\pm}}$	$m_{\eta'}$	m_σ
6.9	−0.9	−0.89	14	24	0.60(2)	0.597(2)	0.596(2)	0.723(3)	0.719(4)	0.65(4)	0.45(6)
6.9	−0.9	−0.88	14	24	0.63(3)	0.6261(18)	0.628(2)	0.749(2)	0.745(3)	0.69(4)	0.51(8)
6.9	−0.9	−0.87	14	24	0.664(17)	0.6510(14)	0.6606(17)	0.7731(19)	0.775(2)	0.77(3)	0.69(14)
6.9	−0.9	−0.85	14	24	⋯	0.6889(19)	0.709(2)	0.813(3)	0.813(4)	⋯	0.51(12)
6.9	−0.9	−0.8	14	24	0.75(2)	0.7563(16)	0.8277(18)	0.879(2)	0.922(3)	0.93(2)	⋯
6.9	−0.9	−0.75	12	24	0.79(3)	0.803(4)	0.921(4)	0.927(6)	1.005(5)	1.04(3)	⋯
6.9	−0.9	−0.7	12	24	0.83(3)	0.833(4)	0.996(3)	0.954(5)	1.073(5)	1.15(3)	⋯

$m_{\pi^0}/m_{\rho^0} \sim 0.85$. Secondly, some meson masses for heavy ensembles sit close to the lattice cutoff and thus could be affected by significant lattice artifacts.

For the heaviest fermion masses, the mass difference between the η' and the π^0 is approximately twice the mass difference between the π^0 and the $\pi^{\pm}$'s. This indicates that the mass differences are driven by the valence fermion masses.

In this regime, the singlet π^0 and the nonsinglet ρ^0 approach an approximate one-flavor theory—see, e.g., Ref. [170] for lattice results on the low-lying spectrum in the SU(2) gauge theory with one Dirac fermion.

In the right panel of Fig. 3, we plot the meson masses as a function of the quark mass ratio, defined through the partially conserved axial current (PCAC) relation. We identify the average quark mass in the flavored pion $\pi^{\pm}$ through the relation

$$m_{\rm avg}^{\rm PCAC} = \lim_{t\to\infty} \frac{1}{2} \frac{\partial_t C_{\gamma_0\gamma_5,\gamma_5}(t)}{C_{\gamma_5}(t)} = \lim_{t\to\infty} \frac{1}{2} \frac{\partial_t \int d^3\vec{x} \langle (\bar{u}(\vec{x},t)\gamma_0\gamma_5 d(\vec{x},t))^\dagger \bar{u}(0)\gamma_5 d(0)\rangle}{\int d^3\vec{x} \langle (\bar{u}(\vec{x},t)\gamma_5 d(\vec{x},t))^\dagger \bar{u}(0)\gamma_5 d(0)\rangle}. \quad (16)$$

The unrenormalized PCAC quark mass ratio m_d/m_u for nondegenerate fermions is extracted by performing an additional measurement of the PCAC average mass at degeneracy. For a detailed discussion of the PCAC relation and different ways to calculate it, we refer to Ref. [239].

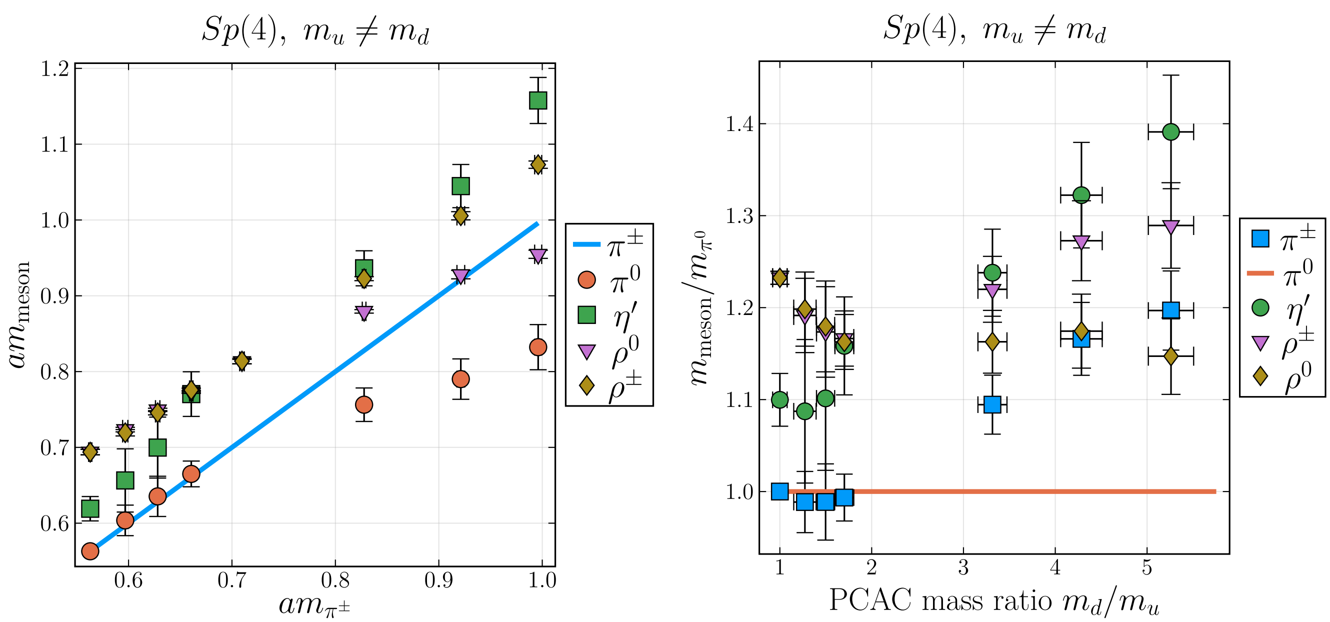

FIG. 3. Masses of the lightest nonsinglet mesons as well as the pseudoscalar singlet meson in the Sp(4) theory with nondegenerate Dirac fermions. We fix the lattice coupling and one of the bare fermion masses to $\beta = 6.9$ and $m_0^{(1)} = -0.9$, respectively, while varying the other bare fermion mass. In the left panel, we display our results as a function of the flavoured pion mass, while in the right panel, we show them as a function of ratio of the PCAC fermion masses in units of the π^0 mass.

C. Scalar singlet in Sp(4) with $N_f = 2$

In the case of the scalar singlet, σ, the signal is consistently worse than for the other states discussed so far. Furthermore, we see signs of finite spacing effects, shown in Fig. 4. For Sp(4) on the coarse $\beta = 6.9$ lattices, we observe a light σ state, of mass comparable to the mass of the π. This pattern persists over the entire mass range considered. On finer lattices, for $\beta = 7.2$, the mass of the σ increases and is heavier than the PNGBs and comparable to the vector meson, though with much larger statistical errors and still below the $\pi\pi$ threshold.

These results suggest the existence of larger finite-spacing effects that affect the mass of the scalar singlet. Yet, some caution should be used because, due to the large noise in our signal, the mass is extracted from much shorter times on the finer lattices and may therefore also be more severely affected by excited-state contamination and possibly other systematics. Nevertheless, even for the finer lattice, the σ state is lighter than its nonsinglet counterpart, suggesting that further studies are still needed. The scalar singlet might be a stable light meson at moderately heavy fermion masses and thus phenomenologically relevant.

D. Comparison to SU(3) with $N_f = 2$

In Fig. 5, we show a compilation of the available data published on the pseudoscalar singlet for the SU(3) theory with $N_f = 2$ (upper panels) as well a comparison of our results for Sp(4) and SU(2) to the available data for SU(3) (lower panels). In some cases, the measurement has been performed using different methods in the analysis, or different operators have been used to study the same mesons (e.g., the mass of the η' has been obtained from pure gluonic operators as well as the usual fermionic operators, or in the case of twisted mass fermions, the nonsinglet mesons include isospin breaking effects) and sets of results are available. In such cases, we have chosen the results that are closest to the standard determination of directly fitting the correlator of a pure fermionic operator. When this was not possible, we quote the largest and smallest values of $m_i \pm \Delta m_i$ of all measurements i and symmetrize the uncertainties. The data depicted in Fig. 5 has been taken from the UKQCD collaborations (denoted by UKQCD1 [202,203] and UKQCD2 [207]); the SESAM/TχL collaboration [204,205]; the *CP*-PACS collaboration [206]; the RBC collaboration using domain-wall fermions [210]; the CLQCD collaboration using Wilson clover fermions on anisotropic lattices [211]; the ETMC collaboration (denoted by ETMC1 [208,209] and ETMC2 [212,213]); and from the analysis of η'-glueball mixing (denoted by Beijing [214]).

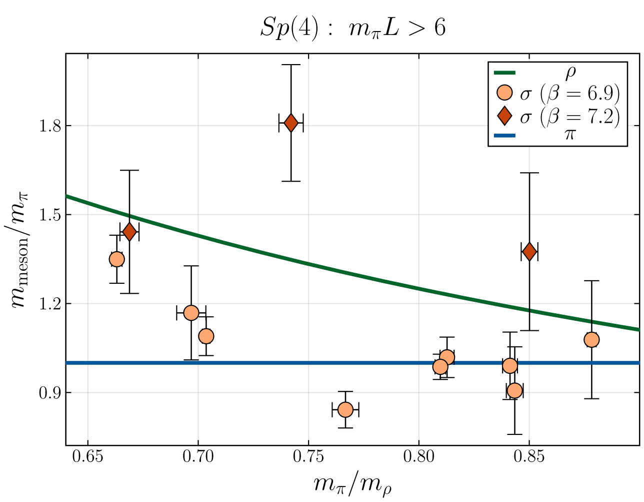

FIG. 4. Mass of the σ meson with degenerate fermions in the Sp(4) theory. We find signs of finite spacing effects even when considering ratios of hadron masses. On the coarser lattice, the scalar singlet appears to be quite light, in some cases, even lighter than the π. For the finer lattice, this changes drastically, and the scalar singlet σ is usually heavier than the vector meson ρ, though still below the two-π threshold. The green solid line $m_\rho/m_\pi = 1/x$ is displayed for reference.

In all but the very lightest ensemble (and one obvious outlier at heavy fermion mass), the vector meson, ρ, is found to be heavier than the pseudoscalar singlet, η'. The authors of Ref. [213] point out that in the lightest ensemble, the ρ particle might be unusually light due to the small number of energy levels below the inelastic threshold in the determination of the $\pi\pi$ phase shift. It is lighter than their extrapolation to the physical point at which $m_\rho = 786(20)$ and even lighter than their extrapolation to the chiral limit. The mass dependence of the η' meson was found to be flat, and an extrapolation in Ref. [212] to the physical point gave $m_{\eta'} = 772(18)$ MeV. This is in contrast to SM QCD where the η' is significantly heavier—the current PDG lists $m_{\eta'}^{\rm PDG} = 957.78(6)$ MeV [240], which is in agreement with recent SU(3), $N_f = 2 + 1$ lattice results of $m_{\eta'} = 929.9(^{47.5}_{21.0})$ [241]. This suggests it is the contribution of the s quark that leads to the heavier mass. This can be understood in a quark model of the pseudoscalar singlet mesons based on approximate $SU(3)_F$ flavor symmetry [242–244], which was applied to early lattice results in [203].

The bottom line of this brief survey is that in the regime of moderately large fermion masses, the pattern of ground state masses observed so far in SU(3) is quite similar, both qualitatively and quantitatively, to our findings in the Sp(4) case as can be seen in the lower panels of Fig. 5. The gauge group and modified chiral structure do not seem to have a very strong impact on mass of the η'.

E. Possible phenomenological implications

Our results provide evidence that the singlet sector, computed for moderately large fermion masses in the Sp(4) theory, is not dissimilar from what is observed in the SU(2) and SU(3) theories coupled to two fundamental fermions. In particular, both pseudoscalar and scalar singlets are light

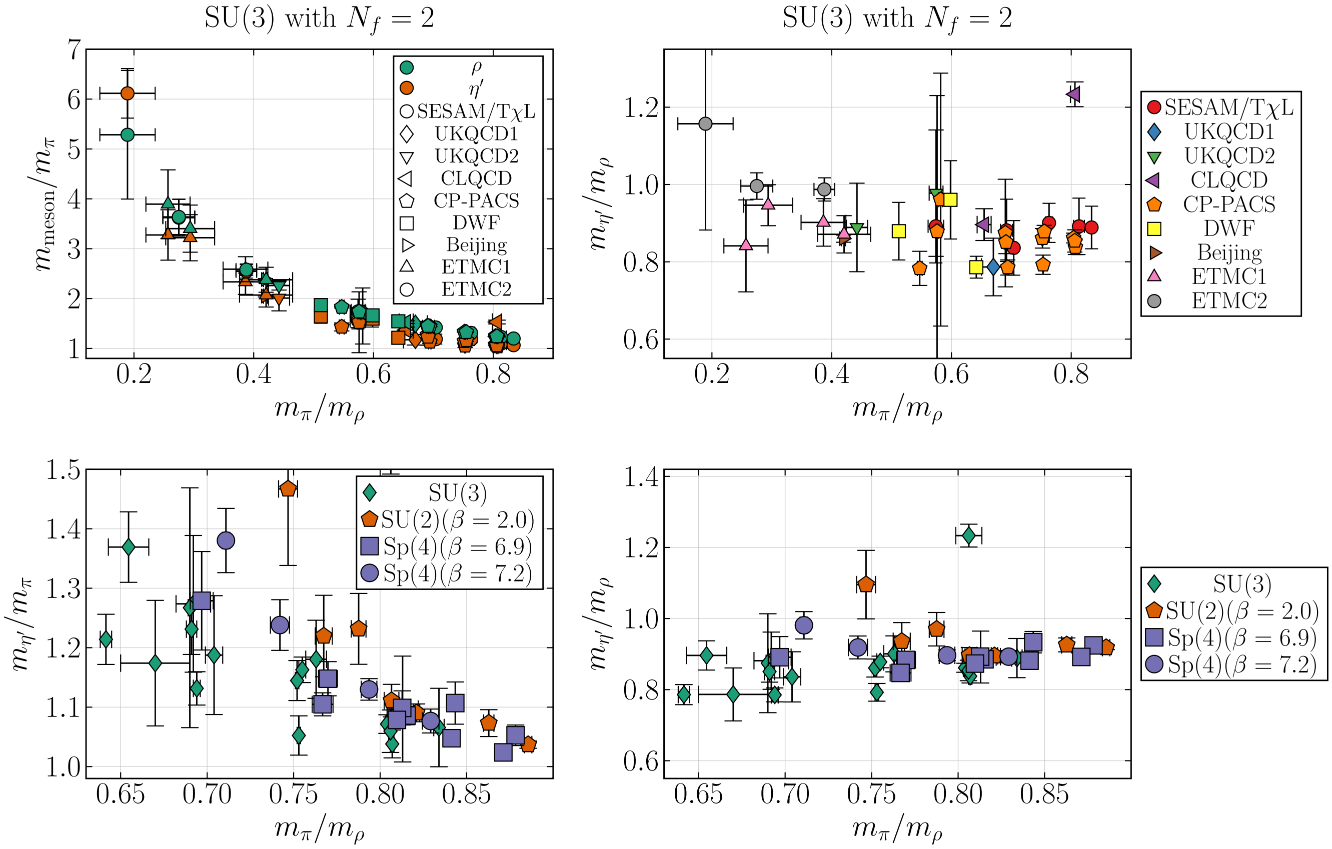

FIG. 5. Comparison to the available lattice data in SU(3) with two fundamental fermions. The upper panels depict all available lattice results in SU(3). In the upper left panel, the green markers denote the vector meson ρ and the orange ones the pseudoscalar singlet η'. The different marker shapes denote the different collaborations. We see that the η' is lighter than the vector mesons almost everywhere. In the upper right panel, we directly plot the ratio $m_{\eta'}/m_\rho$. In the lower panels, we compare the SU(3) results to our Sp(4) and SU(2) data. In the lower left panel, we show the ratio $m_{\eta'}/m_\pi$ as a function of m_π/m_ρ for values of $m_\pi/m_\rho \approx 0.7$ and larger. In the lower right plot, we compare the different results of the ratio $m_{\eta'}/m_\rho$.

enough to be stable against decay into Goldstone bosons, over a fermion-mass range within which also the flavored vector mesons would not decay. We now present a few examples of potential implications for phenomenological models for which these theories can be invoked to yield a short-distance completion.

Firstly, because the flavor singlets are not much heavier than the flavored mesons, if a model of this type were used as part of a hidden valley scenario, or a new dark sector, these states would then only decay via a mediator mechanism into standard model particle, but not strongly, and would be long lived. Their lifetime and branching fractions would be determined by the detailed structure of the coupling to the standard-model fields. They are unlikely to be long lived enough to play a significant role in a model explaining current dark matter density, yet they can easily appear as long-lived particles in experiments [245–248], and hence the existence of a new dark sector containing this theory is experimentally testable.

Other possible observable effects in this context could arise because the singlets can enhance interaction cross-sections, as virtual particles, affecting processes even below production threshold. They can therefore play a relevant role for dark matter self-interactions [249]. Their effect could even affect form factors relevant to direct detection experiments [250]. Depending on details, they could also offer a possibility to create indirect detection signatures in cases of high dark matter densities. Finally, both singlets can serve, together or individually, as a Higgs portal, removing the need for an independent messenger.

In the alternative context of composite Higgs scenarios, in which the PNGBs provide the longitudinal components of the W bosons and Z boson, as well giving rise to the experimentally observed Higgs boson, the pseudoscalar singlet can become a surprisingly strong limiting factor [251]. As its signature is possibly similar to that of the pseudoscalar Higgs in the minimal supersymmetric standard model, or in classes of two-Higgs doublet models, strong exclusion limits already exist, both for a pseudoscalar Higgs heavier and lighter than the standard model Higgs. To avoid these bounds requires one to open up substantially the mass gap between the scalar and pseudoscalar singlets, but in our measurements, we always observe the opposite hierarchy.

V. SUMMARY

We have presented the results of the first dedicated lattice study of flavor singlet meson states in the Sp(4) theory coupled to two (Wilson-Dirac) fundamental dynamical fermions. We have computed the masses of the lightest pseudoscalar and scalar singlets in a portion of parameter space in which the fundamental fermion are moderately heavy. We have considered both the case of degenerate and of nondegenerate masses for the fermions. The continuum limit of this theory, in the range of parameters explored, is of interest because it provides the ultraviolet completion of several proposals for new physics extensions of the standard model, in the contexts of composite Higgs models and strongly interacting dark matter. In order to perform this study, we implemented in our analysis state-of-the-art techniques to account for the contribution of disconnected diagrams to correlation functions involving flavor singlets.

We observe that the qualitative (and to large extent even the quantitative) features of the mass spectrum we find in this Sp(4) theory are similar to those of SU(2) and SU(3) theories with the same field content, in comparable ranges of parameter space. More specifically, the mass range of the singlet states, in particular of the lightest pseudoscalar, is comparable to the masses of the lightest flavored mesons, at least for our choices of fermion masses. This remains true also in the mass-nondegenerate case.

Our findings suggest that the singlet sector cannot be neglected in phenomenological studies of models that have their dynamical, short-distance origin in this theory. However, notwithstanding the technical implementation of several techniques to enhance the signal-to-noise ratio in our measurements, and the comparatively large statistics provided by our numerical ensembles, we have also found that the observables are affected by large lattice artifacts, especially in the case of the scalar singlet. While we have noticed that taking certain ratios of masses reduces drastically the size of such effects, if phenomenological considerations require precision measurements for the mass spectrum, then this would provide strong incentive to further improve this study, in particular in order to better understand the approach to the continuum limit.

On more general and abstract theoretical ground, the similarity of our main results with the $SU(N)$ cases strongly suggests that the altered chiral structure and gauge group has limited impact on the underlying dynamics. On the one hand, this might be expected in a gauge theory with small number of moderately heavy fermions. On the other hand, though, by extending this kind of analysis to different N and/or further gauge groups, we envision to be able to gain quantitative understanding the relevance of gauge dynamics for hadron dynamics beyond group-theoretical, and thus nondynamical, aspects.

The data generated for this manuscript can be downloaded from Ref. [252], and the software used to analyze and present it is similarly available from Ref. [253].

ACKNOWLEDGMENTS

We are grateful to S. Kulkarni for helpful discussions and to the authors of [194,254] for providing access to the smearing code in HiRep prior to publication. F. Z. is supported by the Austrian Science Fund research teams grant STRONG-DM (https://dx.doi.org/10.55776/FG1) (FG1) and acknowledges travel support for part of this work by the city of Graz. The work of E. B. is supported by the UKRI Science and Technology Facilities Council (STFC) Research Software Engineering Fellowship EP/V052489/1, and by the ExaTEPP project No. EP/X017168/1. The work of J. W. L. was supported in part by the National Research Foundation of Korea (NRF) Grant funded by the Korea government(MSIT) (NRF-2018R1C1B3001379) and by IBS under the project code, IBS-R018-D1. The work of B. L. and M. P. has been supported in part by the STFC Consolidated Grant Nos. ST/P00055X/1 and No. ST/T000813/1. B. L. and M. P. received funding from the European Research Council (ERC) under the European Union's Horizon 2020 research and innovation program under Grant Agreement No. 813942. The work of B. L. is further supported in part by the Royal Society Wolfson Research Merit Award No. WM170010 and by the Leverhulme Trust Research Fellowship No. RF-2020-4619. The work of H. H. is supported by the Taiwanese MoST Grant No. 109-2112-M-009-006-MY3. The computations have been partially performed on the HPC cluster of the University of Graz and on the Vienna Scientific Cluster (VSC4), and partially on the DiRAC Data Intensive service at Leicester. The DiRAC Data Intensive service at Leicester is operated by the University of Leicester IT Services, and forms part of the STFC DiRAC HPC Facility [255]. The DiRAC Data Intensive service equipment at Leicester was funded by BEIS capital funding via STFC capital Grant No. ST/K000373/1 and No. ST/R002363/1 and STFC DiRAC Operations grant ST/R001014/1. DiRAC is part of the National e-Infrastructure.

APPENDIX A: CONSTANT CONTRIBUTIONS TO THE CORRELATORS

In Sec. III A, we noted the occurrence of constant terms in the propagators of both the pseudoscalar singlet η' meson and the scalar singlet σ meson. This makes it difficult to determine when the excited states in the meson correlator are sufficiently suppressed and a fit can be performed. As shown in Eqs. (6) and (8), we can circumvent this issue either by direct calculation of $\langle 0|O|0\rangle$ or by performing a numerical derivative. Once we determine the interval $[t_i, t_f]$ where only the ground state contributes, we can also fit the correlator to

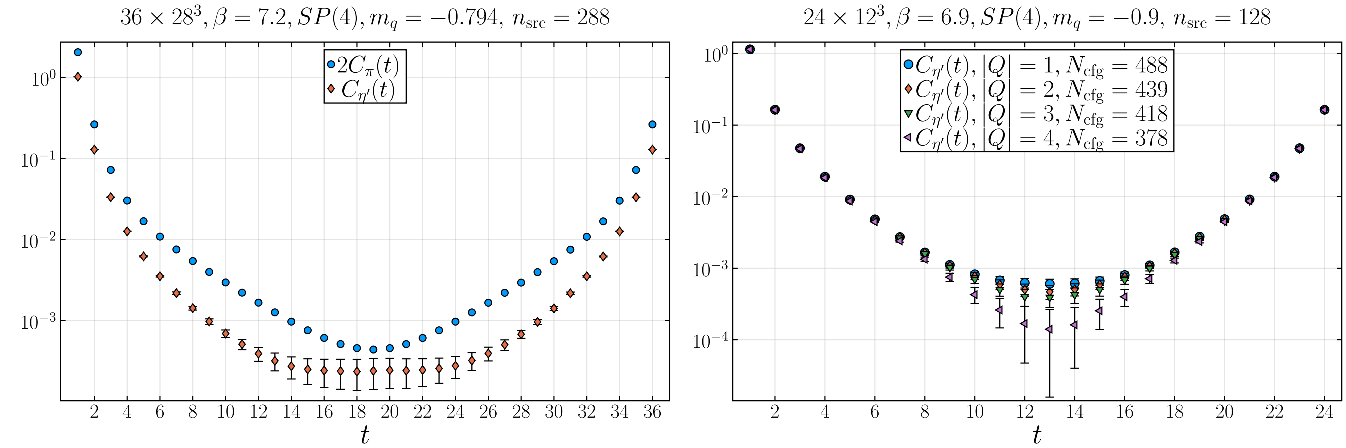

FIG. 6. Left: Correlator of the pseudoscalar nonsinglet π and the pseudoscalar singlet η'. For visual clarity, we multiplied the π correlator by a constant factor of 2. At large times, the singlet correlator shows a constant term, while this is absent for the nonsinglet case. Right: Correlators of the pseudoscalar singlet for fixed values of the topological charge Q. The constant term shows signs of a dependence on Q. While the constant is not significantly different for any two examples shown here, the constant appears to be increasing with $|Q|$.

an exponentially decaying term plus a constant. In Fig. 6, we give an example of the correlator for the flavor singlet, η', and the flavored mesons, π. The flavor-singlet correlator shows a constant term at large Euclidean times, while such a contribution is absent for the π meson. This is expected to occur for the disconnected pieces in a finite volume and at finite statistics if the topological sampling is insufficient [212,234]. Then, the constant takes the form

$$\mathrm{const} \propto \frac{1}{V}\left(\frac{Q^2}{V} - \chi_t - \frac{c_4}{2\chi_t V}\right) + \mathcal{O}(V^{-3}) + \mathcal{O}(e^{-m_\pi |x|}), \quad \text{(A1)}$$

where V denotes the spatial volume of the lattice, χ_t is the topological susceptibility, and c_4 is a coefficient from a saddle-point expansion. Algorithms that provide an ergodic exploration of topological sectors in Yang-Mills theories and are compatible with our prescription for the boundary conditions have recently been introduced (see, e.g., [256–258]). However, they are generally computationally costly, and their adaptation to our model is outside the scope of this work. Hence, in our study, we explore other strategies, based on analyses that account for topological freezing. Therefore, we tried to test the relation in Eq. (A1) by taking our ensemble with the largest statistics (corresponding to the bare parameters $m_0 = -0.90, \beta = 6.9$ on a 24×12^3 lattice), measuring the topological charge Q using the same approach as in Ref. [184], and smoothening the gauge fields using the gradient flow. We then partition our full statistics into sets of configurations with equal topological charge[6] and compute the correlator for the pseudoscalar singlet, η', at fixed Q. We depict examples of the correlators for some values of Q with sufficient statistics in Fig. 6. The constant term arising is never statistically different for any pair of Q's present in this ensemble. However, we see a slight trend toward a larger constant for larger $|Q|$ as expected from Eq. (A1).

In order to test the robustness of our subtraction choice, we report here the mass of the pseudoscalar singlet η' for various techniques. We remind the reader that the results reported in Sec. IV are based on correlators where the connected part is modeled by a single sum of exponentials as in Eq. (8), taking lattice periodicity into account and removing the constant by a numerical derivative. In Table V, we compare this to four alternative methods[7]: (i) direct calculation and subtraction of $\langle 0|O_{\eta'}|0\rangle$, (ii) ignoring the constant and restricting the fit to early time slices, (iii) performing a three-parameter fit of the decaying exponential plus a term modeling the constant,[8] (iv) removing the constant using a numerical derivative but without any modeling of the connected part.

Whenever we obtain a signal without an explicit modeling of the connected pieces, our results agree within errors. The removal of excited state contamination [as used in methods (i), (ii), and (iii)] leads to masses that are generally slightly lighter. The same pattern has been observed in SU(3) [212]. We note that the removal of excited state

[6]In practice, the topological charge is not strictly an integer on a finite lattice in the employed approach as described, for instance, in [184] and references therein. We thus round Q to the closest integer.

[7]We also applied an entirely different method designed for situations with large statistical noise [259]. Also, this approach gave results consistent with those shown in the main part of the paper for both singlets.

[8]This procedure gives the numerical value of the constant as a by-product. We subtract the constant from the correlator and *a posteriori* check that the resulting effective mass shows a plateau.

TABLE V. Determination of the masses of the pseudoscalar singlets using different techniques for removing the constant term in the correlator. We compare the method used in the main part of this work to: (i) Direct calculation and subtraction of $\langle 0|O_{\eta'}|0\rangle$; (ii) Ignoring the constant and restricting the fit to early time-slices; (iii) Performing a three-parameter fit of the decaying exponential plus a term modeling the constant; and (iv) Removing the constant using a numerical derivative but without any modeling of the connected part.

	β	m_0	L	T	$m_{\eta'}$	$m_{\eta'}^{(\mathrm{i})}$	$m_{\eta'}^{(\mathrm{ii})}$	$m_{\eta'}^{(\mathrm{iii})}$	$m_{\eta'}^{(\mathrm{iv})}$
SU(2)	2.0	−0.947	20	32	⋯	⋯	⋯	⋯	⋯
SU(2)	2.0	−0.94	14	24	0.67(6)	0.699(14)	0.572(14)	⋯	0.67(6)
SU(2)	2.0	−0.935	16	32	0.60(3)	0.67(3)	0.61(5)	0.60(3)	⋯
SU(2)	2.0	−0.93	14	24	0.65(3)	⋯	⋯	⋯	0.68(5)
SU(2)	2.0	−0.925	14	24	0.634(16)	⋯	⋯	⋯	0.63(8)
SU(2)	2.0	−0.92	12	24	0.665(9)	⋯	⋯	⋯	0.66(3)
SU(2)	2.0	−0.9	12	24	0.770(16)	⋯	⋯	⋯	0.79(8)
SU(2)	2.0	−0.88	10	20	0.842(5)	0.855(14)	0.855(14)	⋯	⋯
Sp(4)	7.2	−0.799	32	40	⋯	0.37(2)	0.37(2)	⋯	0.57(6)
Sp(4)	7.2	−0.794	28	36	0.397(16)	0.368(12)	0.368(12)	⋯	0.47(7)
Sp(4)	7.2	−0.79	24	36	0.387(13)	⋯	⋯	⋯	0.36(6)
Sp(4)	7.2	−0.78	24	36	0.418(7)	0.43(2)	0.45(2)	⋯	0.43(5)
Sp(4)	7.2	−0.77	24	36	0.456(8)	0.450(6)	0.450(6)	0.459(7)	⋯
Sp(4)	7.2	−0.76	16	36	⋯	0.511(13)	0.512(13)	⋯	0.59(3)
Sp(4)	6.9	−0.924	24	32	⋯	⋯	⋯	⋯	0.60(8)
Sp(4)	6.9	−0.92	24	32	⋯	0.51(4)	0.52(4)	0.486(16)	0.40(6)
Sp(4)	6.9	−0.92	16	32	0.49(3)	0.46(2)	0.46(2)	0.50(2)	0.45(13)
Sp(4)	6.9	−0.91	16	32	0.560(14)	0.59(4)	0.59(4)	0.560(13)	0.59(4)
Sp(4)	6.9	−0.91	14	24	0.541(9)	0.58(3)	0.58(3)	⋯	⋯
Sp(4)	6.9	−0.9	16	32	0.611(9)	⋯	⋯	⋯	0.63(3)
Sp(4)	6.9	−0.9	14	24	0.619(16)	0.614(12)	0.615(12)	0.620(9)	0.63(3)
Sp(4)	6.9	−0.9	12	24	0.610(6)	0.620(15)	0.620(15)	0.612(5)	⋯
Sp(4)	6.9	−0.89	14	24	0.69(2)	0.680(16)	0.681(16)	0.69(2)	0.72(4)
Sp(4)	6.9	−0.89	12	24	0.661(9)	0.660(5)	0.660(5)	0.660(10)	⋯
Sp(4)	6.9	−0.87	12	24	0.782(13)	0.80(4)	0.80(4)	⋯	0.80(2)
Sp(4)	6.9	−0.87	10	20	0.764(9)	0.763(6)	0.763(6)	⋯	⋯

contaminations should not be confused with the removal of the constant contribution to the correlator, as discussed earlier. The explicit calculation of the constant $\langle 0|O_{\eta'}|0\rangle$ in Eq. (8) does not quantitatively capture the constant in the correlator. The results are almost indistinguishable from not taking the constant into account. For some ensembles (e.g., Sp(4) with $\beta = 7.2$), these methods appear to underestimate the meson mass. This is a result of combining the modeling of the connected piece with an insufficient subtraction of the constant. Due to the absence of connected excited states in the correlator, the effective mass is increasing at small t, while for large t, the constant leads to a decrease of the effective masses. This can lead to the formation of an apparent plateau in the effective mass and thus to a possible underestimation of the meson mass. Overall, we conclude that methods (ii) and (iii) do not appear sufficiently reliable. Modeling the constant as an additional fit parameter did not lead to any significant improvements. In most cases, we cannot extract a reliable signal. In the few cases where this is possible, the constant term is quantitatively small, and this method agrees with the others while providing no improvement at the cost of an additional fit parameter.

We conclude that the method used throughout the main part of this work has proven to be the most reliable approach among the options considered here. Its results are always consistent with forgoing the explicit removal of subtracted states, and the removal of the additional constant through taking the derivative avoids any further estimations of the topological constant terms at the expense of a shorter plateau in the effective masses and thus, a smaller interval for fitting the correlator.

We find a different behavior for the scalar singlet. The constant term is not related to an insufficient sampling of all topological sectors but arises due to the vacuum quantum numbers of the scalar singlet. In addition, the modeling of the connected pieces is less important since the nonsinglet state appears generally heavier than the singlet states and the connected pieces show a stronger exponential decay. In this case, the direct estimation of the constant term $\langle 0|O_\sigma|0\rangle$ in Eq. (8) appears to be quantitatively reliable. Still, in some cases, the modeling of the connected pieces can extend the plateau in the effective mass to lower time slices t. Since the constant is several orders of magnitude larger than the actual signal of the σ state, a direct modeling of it as a fit parameter is infeasible, and the constant can also not be

TABLE VI. Results for the masses of the scalar singlet σ using our standard approach of a numerical derivative as well as (i) both a numerical derivative and a direct calculation of the vacuum term $\langle 0|O_\sigma|0\rangle$, (ii) only direct calculation of the vacuum term, and (iii) a numerical derivative without an explicit subtraction of excited states in the connected piece when possible.

	β	m_0	L	T	m_σ	$m_\sigma^{(i)}$	$m_\sigma^{(ii)}$	$m_\sigma^{(iii)}$
SU(2)	2.0	−0.947	20	32	0.53(4)	0.53(3)	0.58(5)	0.54(4)
SU(2)	2.0	−0.94	14	24	⋯	0.64(5)	0.61(4)	0.64(5)
SU(2)	2.0	−0.935	16	32	⋯	0.47(10)	0.55(8)	0.47(10)
SU(2)	2.0	−0.93	14	24	⋯	⋯	0.62(9)	⋯
SU(2)	2.0	−0.925	14	24	⋯	⋯	⋯	⋯
SU(2)	2.0	−0.92	12	24	⋯	0.71(7)	0.75(13)	0.72(7)
SU(2)	2.0	−0.9	12	24	⋯	⋯	⋯	⋯
SU(2)	2.0	−0.88	10	20	⋯	⋯	⋯	⋯
Sp(4)	7.2	−0.799	32	40	0.36(5)	0.35(8)	0.41(4)	0.38(8)
Sp(4)	7.2	−0.794	28	36	⋯	0.55(8)	⋯	0.55(8)
Sp(4)	7.2	−0.79	24	36	0.56(6)	0.56(6)	0.48(7)	0.65(12)
Sp(4)	7.2	−0.78	24	36	⋯	⋯	0.55(6)	⋯
Sp(4)	7.2	−0.77	24	36	⋯	⋯	⋯	⋯
Sp(4)	7.2	−0.76	16	36	0.64(12)	0.64(7)	⋯	⋯
Sp(4)	6.9	−0.924	24	32	0.46(3)	0.46(3)	0.45(3)	0.48(7)
Sp(4)	6.9	−0.92	24	32	0.42(2)	0.43(3)	0.45(3)	⋯
Sp(4)	6.9	−0.92	16	32	0.45(6)	0.40(8)	0.42(7)	0.37(11)
Sp(4)	6.9	−0.91	16	32	⋯	⋯	⋯	0.71(8)
Sp(4)	6.9	−0.91	14	24	0.41(3)	0.41(3)	⋯	⋯
Sp(4)	6.9	−0.9	16	32	⋯	⋯	⋯	⋯
Sp(4)	6.9	−0.9	14	24	0.57(4)	0.56(4)	0.48(5)	0.51(10)
Sp(4)	6.9	−0.9	12	24	0.55(2)	0.56(4)	⋯	0.57(3)
Sp(4)	6.9	−0.89	14	24	0.57(9)	0.56(9)	0.61(9)	0.59(9)
Sp(4)	6.9	−0.89	12	24	0.62(7)	⋯	0.64(4)	⋯
Sp(4)	6.9	−0.87	12	24	0.80(15)	0.76(11)	⋯	0.72(7)
Sp(4)	6.9	−0.87	10	20	⋯	0.70(6)	⋯	⋯

ignored in the analysis. In Table VI, we compare the approach used in the main part of this paper to (i) both a numerical derivative and a direct calculation and subsequent subtraction of the vacuum term $\langle 0|O_\sigma|0\rangle$, (ii) only direct subtraction of the vacuum terms as in [215], (iii) a numerical derivative without an explicit subtraction of excited states in the connected pieces and without a direct subtraction of $\langle 0|O_\sigma|0\rangle$.

APPENDIX B: COMPARISON BETWEEN EXCITED STATE SUBTRACTION AND SMEARED CONNECTED DIAGRAMS

In Sec. III B, we noted that the signal of the singlet mesons can be extended to smaller time separations, t, if we replace its connected contribution by approximating it with a single exponential term having the energy of the nonsinglet meson. This removes all the excited state contaminations of the connected piece.

A similar effect can be obtained by using smearing techniques on the connected piece. This can increase the overlap of the source operator with the ground state of the nonsinglet and reduce the contribution of excited states. Recently, this approach has been implemented, tested, and shown to work in Sp(4) gauge theories [194]. These developments allow us to compare our excited-state subtraction technique.[9]

In order to compare the two techniques, we need to apply smearing to only the connected piece. However, the use of smearing techniques leads to an overall change of normalization. Applying Wuppertal smearing [260] with N_1 steps at the source and N_2 steps at the sink leads to an asymptotic correlator of the form

$$C_{N_1,N_2}(t\to\infty) = \alpha_{N_1}\alpha_{N_2}e^{-m_{\rm conn}t}, \tag{B1}$$

where the normalization of unsmeared point sources is recovered for the choice of the parameters $\alpha_{N_1} = \alpha_{N_2} = \alpha_0$. We consider two sets of correlators with the smearing steps $(N_1, N_2) = (N, 0)$ and $(N_1, N_2) = (N, N)$, to restore the normalization as the point source. We define a new correlator

$$C^{\rm smeared}_{\rm conn}(t) \equiv \frac{C_{N,0}(t)^2}{C_{N,N}(t)}, \tag{B2}$$

[9] We thank the authors of [194,254] for performing smeared measurements on a set of our configurations for comparison prior to publication.

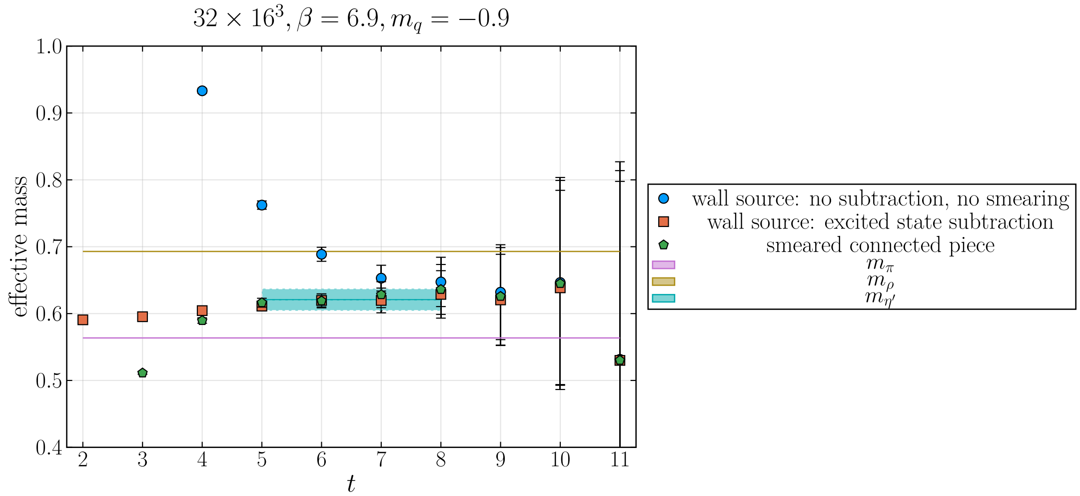

FIG. 7. Comparison between excited state subtraction (orange squares), obtained by modeling the connected part of the correlator as a single exponential term, with smeared operators (green pentagon), on a preliminary set of configurations, for a single ensemble. For reference, we also plot the correlator without excited state subtraction and without smearing (blue circles).

by squaring the connected correlator with N steps of source smearing and no sink smearing and divide that by the connected correlator with an equal amount of smearing steps at both the source and the sink. This correlator has the same large-t behavior and the same normalization as a nonsmeared one. From this, we then construct the full correlator of the singlet meson. In Fig. 7, we compare the full singlet correlator obtained from Eq. (B2) using Wuppertal smearing with $N = 60$ smearing steps, to the correlator obtained using the single-exponential modeling and subtraction of the connected piece. We see that the subtracted correlator and the smeared correlator agree remarkably well in the interesting plateau region.

[1] D. B. Kaplan and H. Georgi, $SU(2) \times U(1)$ breaking by vacuum misalignment, Phys. Lett. **136B**, 183 (1984).
[2] H. Georgi and D. B. Kaplan, Composite Higgs and custodial SU(2), Phys. Lett. **145B**, 216 (1984).
[3] M. J. Dugan, H. Georgi, and D. B. Kaplan, Anatomy of a composite Higgs model, Nucl. Phys. **B254**, 299 (1985).
[4] G. Panico and A. Wulzer, The composite Nambu-Goldstone Higgs, Lect. Notes Phys. **913**, 1 (2016).
[5] O. Witzel, Review on composite Higgs models, Proc. Sci., LATTICE2018 (**2019**) 006 [arXiv:1901.08216].
[6] G. Cacciapaglia, C. Pica, and F. Sannino, Fundamental composite dynamics: A review, Phys. Rep. **877**, 1 (2020).
[7] G. Ferretti and D. Karateev, Fermionic UV completions of composite Higgs models, J. High Energy Phys. 03 (2014) 077.
[8] G. Ferretti, Gauge theories of partial compositeness: Scenarios for Run-II of the LHC, J. High Energy Phys. 06 (2016) 107.
[9] G. Cacciapaglia, G. Ferretti, T. Flacke, and H. Serôdio, Light scalars in composite Higgs models, Front. Phys. **7**, 22 (2019).
[10] E. Katz, A. E. Nelson, and D. G. E. Walker, The intermediate Higgs, J. High Energy Phys. 08 (2005) 074.
[11] R. Barbieri, B. Bellazzini, V. S. Rychkov, and A. Varagnolo, The Higgs boson from an extended symmetry, Phys. Rev. D **76**, 115008 (2007).
[12] P. Lodone, Vector-like quarks in a 'composite' Higgs model, J. High Energy Phys. 12 (2008) 029.
[13] B. Gripaios, A. Pomarol, F. Riva, and J. Serra, Beyond the minimal composite Higgs model, J. High Energy Phys. 04 (2009) 070.
[14] J. Mrazek, A. Pomarol, R. Rattazzi, M. Redi, J. Serra, and A. Wulzer, The other natural two Higgs doublet model, Nucl. Phys. **B53**, 1 (2011).
[15] D. Marzocca, M. Serone, and J. Shu, General composite Higgs models, J. High Energy Phys. 08 (2012) 013.
[16] J. Barnard, T. Gherghetta, and T. S. Ray, UV descriptions of composite Higgs models without elementary scalars, J. High Energy Phys. 02 (2014) 002.
[17] C. Grojean, O. Matsedonskyi, and G. Panico, Light top partners and precision physics, J. High Energy Phys. 10 (2013) 160.

[18] G. Cacciapaglia and F. Sannino, Fundamental composite (Goldstone) Higgs dynamics, J. High Energy Phys. 04 (2014) 111.
[19] G. Ferretti, UV completions of partial compositeness: The case for a SU(4) gauge group, J. High Energy Phys. 06 (2014) 142.
[20] A. Arbey, G. Cacciapaglia, H. Cai, A. Deandrea, S. Le Corre, and F. Sannino, Fundamental composite electroweak dynamics: Status at the LHC, Phys. Rev. D **95**, 015028 (2017).
[21] G. Cacciapaglia, H. Cai, A. Deandrea, T. Flacke, S. J. Lee, and A. Parolini, Composite scalars at the LHC: The Higgs, the sextet and the octet, J. High Energy Phys. 11 (2015) 201.
[22] F. Feruglio, B. Gavela, K. Kanshin, P. A. N. Machado, S. Rigolin, and S. Saa, The minimal linear sigma model for the Goldstone Higgs, J. High Energy Phys. 06 (2016) 038.
[23] T. DeGrand, M. Golterman, E. T. Neil, and Y. Shamir, One-loop chiral perturbation theory with two fermion representations, Phys. Rev. D **94**, 025020 (2016).
[24] S. Fichet, G. von Gersdorff, E. Pontón, and R. Rosenfeld, The excitation of the global symmetry-breaking vacuum in composite Higgs models, J. High Energy Phys. 09 (2016) 158.
[25] J. Galloway, A. L. Kagan, and A. Martin, A UV complete partially composite-pNGB Higgs, Phys. Rev. D **95**, 035038 (2017).
[26] A. Agugliaro, O. Antipin, D. Becciolini, S. De Curtis, and M. Redi, UV complete composite Higgs models, Phys. Rev. D **95**, 035019 (2017).
[27] A. Belyaev, G. Cacciapaglia, H. Cai, G. Ferretti, T. Flacke, A. Parolini, and H. Serodio, Di-boson signatures as standard candles for partial compositeness, J. High Energy Phys. 01 (2017) 094; J. High Energy Phys. 12 (2017) 88.
[28] C. Csaki, T. Ma, and J. Shu, Maximally symmetric composite Higgs models, Phys. Rev. Lett. **119**, 131803 (2017).
[29] M. Chala, G. Durieux, C. Grojean, L. de Lima, and O. Matsedonskyi, Minimally extended SILH, J. High Energy Phys. 06 (2017) 088.
[30] M. Golterman and Y. Shamir, Effective potential in ultraviolet completions for composite Higgs models, Phys. Rev. D **97**, 095005 (2018).
[31] C. Csáki, T. Ma, and J. Shu, Trigonometric parity for composite Higgs models, Phys. Rev. Lett. **121**, 231801 (2018).
[32] T. Alanne, D. Buarque Franzosi, and M. T. Frandsen, A partially composite Goldstone Higgs, Phys. Rev. D **96**, 095012 (2017).
[33] T. Alanne, D. Buarque Franzosi, M. T. Frandsen, M. L. A. Kristensen, A. Meroni, and M. Rosenlyst, Partially composite Higgs models: Phenomenology and RG analysis, J. High Energy Phys. 01 (2018) 051.
[34] F. Sannino, P. Stangl, D. M. Straub, and A. E. Thomsen, Flavor physics and flavor anomalies in minimal fundamental partial compositeness, Phys. Rev. D **97**, 115046 (2018).
[35] T. Alanne, N. Bizot, G. Cacciapaglia, and F. Sannino, Classification of NLO operators for composite Higgs models, Phys. Rev. D **97**, 075028 (2018).
[36] N. Bizot, G. Cacciapaglia, and T. Flacke, Common exotic decays of top partners, J. High Energy Phys. 06 (2018) 065.
[37] C. Cai, G. Cacciapaglia, and H.-H. Zhang, Vacuum alignment in a composite 2HDM, J. High Energy Phys. 01 (2019) 130.
[38] A. Agugliaro, G. Cacciapaglia, A. Deandrea, and S. De Curtis, Vacuum misalignment and pattern of scalar masses in the SU(5)/SO(5) composite Higgs model, J. High Energy Phys. 02 (2019) 089.
[39] G. Cacciapaglia, T. Ma, S. Vatani, and Y. Wu, Towards a fundamental safe theory of composite Higgs and dark matter, Eur. Phys. J. C **80**, 1088 (2020).
[40] H. Gertov, A. E. Nelson, A. Perko, and D. G. E. Walker, Lattice-friendly gauge completion of a composite Higgs with top partners, J. High Energy Phys. 02 (2019) 181.
[41] V. Ayyar, M. F. Golterman, D. C. Hackett, W. Jay, E. T. Neil, Y. Shamir, and B. Svetitsky, Radiative contribution to the composite-Higgs potential in a two-representation lattice model, Phys. Rev. D **99**, 094504 (2019).
[42] G. Cacciapaglia, H. Cai, A. Deandrea, and A. Kushwaha, Composite Higgs and dark matter model in SU(6)/SO(6)., J. High Energy Phys. 10 (2019) 035.
[43] D. Buarque Franzosi and G. Ferretti, Anomalous dimensions of potential top-partners, SciPost Phys. **7**, 027 (2019).
[44] G. Cacciapaglia, S. Vatani, and C. Zhang, Composite Higgs meets planck scale: Partial compositeness from partial unification, Phys. Lett. B **815**, 136177 (2021).
[45] G. Cacciapaglia, A. Deandrea, T. Flacke, and A. M. Iyer, Gluon-photon signatures for color octet at the LHC (and beyond)., J. High Energy Phys. 05 (2020) 027.
[46] Z.-Y. Dong, C.-S. Guan, T. Ma, J. Shu, and X. Xue, UV completed composite Higgs model with heavy composite partners, Phys. Rev. D **104**, 035013 (2021).
[47] G. Cacciapaglia, T. Flacke, M. Kunkel, and W. Porod, Phenomenology of unusual top partners in composite Higgs models, J. High Energy Phys. 02 (2022) 208.
[48] A. Banerjee, D. B. Franzosi, and G. Ferretti, modeling vector-like quarks in partial compositeness framework, J. High Energy Phys. 03 (2022) 200.
[49] R. Contino, Y. Nomura, and A. Pomarol, Higgs as a holographic pseudo Goldstone boson, Nucl. Phys. **B671**, 148 (2003).
[50] K. Agashe, R. Contino, and A. Pomarol, The minimal composite Higgs model, Nucl. Phys. **B719**, 165 (2005).
[51] K. Agashe and R. Contino, The minimal composite Higgs model and electroweak precision tests, Nucl. Phys. **B742**, 59 (2006).
[52] K. Agashe, R. Contino, L. Da Rold, and A. Pomarol, A custodial symmetry for $Zb\bar{b}$, Phys. Lett. B **641**, 62 (2006).
[53] R. Contino, L. Da Rold, and A. Pomarol, Light custodians in natural composite Higgs models, Phys. Rev. D **75**, 055014 (2007).
[54] A. Falkowski and M. Perez-Victoria, Electroweak breaking on a soft wall, J. High Energy Phys. 12 (2008) 107.
[55] R. Contino, The Higgs as a Composite Nambu-Goldstone Boson, in *Theoretical Advanced Study Institute in Elementary Particle Physics: Physics of the Large and the Small*

(World Scientific, Singapore, 2011), pp. 235–306, arXiv:1005.4269.
[56] R. Contino, D. Marzocca, D. Pappadopulo, and R. Rattazzi, On the effect of resonances in composite Higgs phenomenology, J. High Energy Phys. 10 (2011) 081.
[57] F. Caracciolo, A. Parolini, and M. Serone, UV completions of composite Higgs models with partial compositeness, J. High Energy Phys. 02 (2013) 066.
[58] J. Erdmenger, N. Evans, W. Porod, and K. S. Rigatos, Gauge/gravity dynamics for composite Higgs models and the top mass, Phys. Rev. Lett. **126**, 071602 (2021).
[59] J. Erdmenger, N. Evans, W. Porod, and K. S. Rigatos, Gauge/gravity dual dynamics for the strongly coupled sector of composite Higgs models, J. High Energy Phys. 02 (2021) 058.
[60] D. Elander, M. Frigerio, M. Knecht, and J.-L. Kneur, Holographic models of composite Higgs in the Veneziano limit. Part I. Bosonic sector, J. High Energy Phys. 03 (2021) 182.
[61] D. Elander, M. Frigerio, M. Knecht, and J.-L. Kneur, Holographic models of composite Higgs in the Veneziano limit. Part II. Fermionic sector, J. High Energy Phys. 05 (2022) 066.
[62] D. Elander and M. Piai, Towards top-down holographic composite Higgs: Minimal coset from maximal supergravity, J. High Energy Phys. 03 (2022) 049.
[63] D. Elander, A. Fatemiabhari, and M. Piai, Toward composite Higgs: Minimal coset from a regular bottom-up holographic model, Phys. Rev. D **107**, 115021 (2023).
[64] Y. Hochberg, E. Kuflik, T. Volansky, and J. G. Wacker, Mechanism for thermal relic dark matter of strongly interacting massive particles, Phys. Rev. Lett. **113**, 171301 (2014).
[65] Y. Hochberg, E. Kuflik, H. Murayama, T. Volansky, and J. G. Wacker, Model for thermal relic dark matter of strongly interacting massive particles, Phys. Rev. Lett. **115**, 021301 (2015).
[66] Y. Hochberg, E. Kuflik, and H. Murayama, SIMP spectroscopy, J. High Energy Phys. 05 (2016) 090.
[67] M. Hansen, K. Langæble, and F. Sannino, SIMP model at NNLO in chiral perturbation theory, Phys. Rev. D **92**, 075036 (2015).
[68] N. Bernal, X. Chu, and J. Pradler, Simply split strongly interacting massive particles, Phys. Rev. D **95**, 115023 (2017).
[69] A. Berlin, N. Blinov, S. Gori, P. Schuster, and N. Toro, Cosmology and accelerator tests of strongly interacting dark matter, Phys. Rev. D **97**, 055033 (2018).
[70] N. Bernal, X. Chu, S. Kulkarni, and J. Pradler, Self-interacting dark matter without prejudice, Phys. Rev. D **101**, 055044 (2020).
[71] Y.-D. Tsai, R. McGehee, and H. Murayama, Resonant self-interacting dark matter from dark QCD, Phys. Rev. Lett. **128**, 172001 (2022).
[72] D. Kondo, R. McGehee, T. Melia, and H. Murayama, Linear sigma dark matter, J. High Energy Phys. 09 (2022) 041.
[73] N. Bernal and X. Chu, $\mathbb{Z}_2$ SIMP dark matter, J. Cosmol. Astropart. Phys. 01 (2016) 006.
[74] W. J. G. de Blok, The core-cusp problem, Adv. Astron. **2010**, 789293 (2010).
[75] M. Boylan-Kolchin, J. S. Bullock, and M. Kaplinghat, Too big to fail? The puzzling darkness of massive Milky Way subhaloes, Mon. Not. R. Astron. Soc. **415**, L40 (2011).
[76] N. Seto, S. Kawamura, and T. Nakamura, Possibility of direct measurement of the acceleration of the universe using 0.1-Hz band laser interferometer gravitational wave antenna in space, Phys. Rev. Lett. **87**, 221103 (2001).
[77] S. Kawamura *et al.*, The Japanese space gravitational wave antenna DECIGO, Classical Quantum Gravity **23**, S125 (2006).
[78] J. Crowder and N. J. Cornish, Beyond LISA: Exploring future gravitational wave missions, Phys. Rev. D **72**, 083005 (2005).
[79] V. Corbin and N. J. Cornish, Detecting the cosmic gravitational wave background with the big bang observer, Classical Quantum Gravity **23**, 2435 (2006).
[80] G. M. Harry, P. Fritschel, D. A. Shaddock, W. Folkner, and E. S. Phinney, Laser interferometry for the big bang observer, Classical Quantum Gravity **23**, 4887 (2006); **23**, 7361(E) (2006).
[81] S. Hild *et al.*, Sensitivity studies for third-generation gravitational wave observatories, Classical Quantum Gravity **28**, 094013 (2011).
[82] K. Yagi and N. Seto, Detector configuration of DECIGO/BBO and identification of cosmological neutron-star binaries, Phys. Rev. D **83**, 044011 (2011); **95**, 109901 (E) (2017).
[83] B. Sathyaprakash *et al.*, Scientific objectives of Einstein telescope, Classical Quantum Gravity **29**, 124013 (2012); **30**, 079501(E) (2013).
[84] E. Thrane and J. D. Romano, Sensitivity curves for searches for gravitational-wave backgrounds, Phys. Rev. D **88**, 124032 (2013).
[85] C. Caprini *et al.*, Science with the space-based interferometer eLISA. II: Gravitational waves from cosmological phase transitions, J. Cosmol. Astropart. Phys. 04 (2016) 001.
[86] P. Amaro-Seoane *et al.* (LISA Collaboration), Laser Interferometer Space Antenna, arXiv:1702.00786.
[87] B. P. Abbott *et al.* (LIGO Scientific Collaboration), Exploring the sensitivity of next generation gravitational wave detectors, Classical Quantum Gravity **34**, 044001 (2017).
[88] S. Isoyama, H. Nakano, and T. Nakamura, Multiband gravitational-wave astronomy: Observing binary inspirals with a decihertz detector, B-DECIGO, Prog. Theor. Exp. Phys. **2018**, 073E01 (2018).
[89] J. Baker *et al.*, The laser interferometer space antenna: Unveiling the millihertz gravitational wave sky, arXiv:1907.06482.
[90] V. Brdar, A. J. Helmboldt, and J. Kubo, Gravitational waves from first-order phase transitions: LIGO as a window to unexplored Seesaw scales, J. Cosmol. Astropart. Phys. 02 (2019) 021.
[91] D. Reitze *et al.*, Cosmic Explorer: The U.S. Contribution to gravitational-wave astronomy beyond LIGO, Bull. Am. Astron. Soc. **51**, 035 (2019).

[92] C. Caprini et al., Detecting gravitational waves from cosmological phase transitions with LISA: An update, J. Cosmol. Astropart. Phys. 03 (2020) 024.

[93] M. Maggiore et al., Science case for the Einstein Telescope, J. Cosmol. Astropart. Phys. 03 (2020) 050.

[94] E. Witten, Cosmic separation of phases, Phys. Rev. D **30**, 272 (1984).

[95] M. Kamionkowski, A. Kosowsky, and M. S. Turner, Gravitational radiation from first order phase transitions, Phys. Rev. D **49**, 2837 (1994).

[96] B. Allen, The stochastic gravity wave background: Sources and detection, in *Les Houches School of Physics: Astrophysical Sources of Gravitational Radiation* (Cambridge University Press, Cambridge, England, 1996), pp. 373–417.

[97] P. Schwaller, Gravitational waves from a dark phase transition, Phys. Rev. Lett. **115**, 181101 (2015).

[98] D. Croon, V. Sanz, and G. White, Model discrimination in gravitational wave spectra from dark phase transitions, J. High Energy Phys. 08 (2018) 203.

[99] N. Christensen, Stochastic gravitational wave backgrounds, Rep. Prog. Phys. **82**, 016903 (2019).

[100] W.-C. Huang, M. Reichert, F. Sannino, and Z.-W. Wang, Testing the dark SU(N) Yang-Mills theory confined landscape: From the lattice to gravitational waves, Phys. Rev. D **104**, 035005 (2021).

[101] J. Halverson, C. Long, A. Maiti, B. Nelson, and G. Salinas, Gravitational waves from dark Yang-Mills sectors, J. High Energy Phys. 05 (2021) 154.

[102] Z. Kang, J. Zhu, and S. Matsuzaki, Dark confinement-deconfinement phase transition: A roadmap from Polyakov loop models to gravitational waves, J. High Energy Phys. 09 (2021) 060.

[103] M. Reichert, F. Sannino, Z.-W. Wang, and C. Zhang, Dark confinement and chiral phase transitions: Gravitational waves vs matter representations, J. High Energy Phys. 01 (2022) 003.

[104] M. Reichert and Z.-W. Wang, Gravitational waves from dark composite dynamics, EPJ Web Conf. **274**, 08003 (2022).

[105] C. N. Leung, S. T. Love, and W. A. Bardeen, Spontaneous symmetry breaking in scale invariant quantum electrodynamics, Nucl. Phys. **B273**, 649 (1986).

[106] W. A. Bardeen, C. N. Leung, and S. T. Love, The dilaton and chiral symmetry breaking, Phys. Rev. Lett. **56**, 1230 (1986).

[107] K. Yamawaki, M. Bando, and K.-i. Matumoto, Scale invariant technicolor model and a technidilaton, Phys. Rev. Lett. **56**, 1335 (1986).

[108] W. D. Goldberger, B. Grinstein, and W. Skiba, Distinguishing the Higgs boson from the dilaton at the Large Hadron Collider, Phys. Rev. Lett. **100**, 111802 (2008).

[109] D. K. Hong, S. D. H. Hsu, and F. Sannino, Composite Higgs from higher representations, Phys. Lett. B **597**, 89 (2004).

[110] D. D. Dietrich, F. Sannino, and K. Tuominen, Light composite Higgs from higher representations versus electroweak precision measurements: Predictions for CERN LHC, Phys. Rev. D **72**, 055001 (2005).

[111] M. Hashimoto and K. Yamawaki, Techni-dilaton at conformal edge, Phys. Rev. D **83**, 015008 (2011).

[112] T. Appelquist and Y. Bai, A light dilaton in walking gauge theories, Phys. Rev. D **82**, 071701 (2010).

[113] L. Vecchi, Phenomenology of a light scalar: The dilaton, Phys. Rev. D **82**, 076009 (2010).

[114] Z. Chacko and R. K. Mishra, Effective theory of a light dilaton, Phys. Rev. D **87**, 115006 (2013).

[115] B. Bellazzini, C. Csaki, J. Hubisz, J. Serra, and J. Terning, A Higgslike dilaton, Eur. Phys. J. C **73**, 2333 (2013).

[116] B. Bellazzini, C. Csaki, J. Hubisz, J. Serra, and J. Terning, A naturally light dilaton and a small cosmological constant, Eur. Phys. J. C **74**, 2790 (2014).

[117] T. Abe, R. Kitano, Y. Konishi, K.-y. Oda, J. Sato, and S. Sugiyama, Minimal dilaton model, Phys. Rev. D **86**, 115016 (2012).

[118] E. Eichten, K. Lane, and A. Martin, A Higgs impostor in low-scale technicolor, arXiv:1210.5462.

[119] P. Hernandez-Leon and L. Merlo, Distinguishing A Higgs-like dilaton scenario with a complete bosonic effective field theory basis, Phys. Rev. D **96**, 075008 (2017).

[120] J. Cruz Rojas, D. K. Hong, S. H. Im, and M. Järvinen, Holographic light dilaton at the conformal edge, J. High Energy Phys. 05 (2023) 204.

[121] A. A. Migdal and M. A. Shifman, Dilaton effective Lagrangian in gluodynamics, Phys. Lett. **114B**, 445 (1982).

[122] S. Coleman, *Aspects of Symmetry: Selected Erice Lectures* (Cambridge University Press, Cambridge, UK, 1985).

[123] S. Matsuzaki and K. Yamawaki, Dilaton chiral perturbation theory: Determining the mass and decay constant of the technidilaton on the lattice, Phys. Rev. Lett. **113**, 082002 (2014).

[124] M. Golterman and Y. Shamir, Low-energy effective action for pions and a dilatonic meson, Phys. Rev. D **94**, 054502 (2016).

[125] A. Kasai, K.-i. Okumura, and H. Suzuki, A dilaton-pion mass relation, arXiv:1609.02264.

[126] M. Hansen, K. Langæble, and F. Sannino, Extending chiral perturbation theory with an isosinglet scalar, Phys. Rev. D **95**, 036005 (2017).

[127] M. Golterman and Y. Shamir, Effective pion mass term and the trace anomaly, Phys. Rev. D **95**, 016003 (2017).

[128] T. Appelquist, J. Ingoldby, and M. Piai, Dilaton EFT framework for lattice data, J. High Energy Phys. 07 (2018) 035.

[129] T. Appelquist, J. Ingoldby, and M. Piai, Analysis of a dilaton EFT for lattice data, J. High Energy Phys. 03 (2017) 039.

[130] M. Golterman and Y. Shamir, Large-mass regime of the dilaton-pion low-energy effective theory, Phys. Rev. D **98**, 056025 (2018).

[131] O. Catà and C. Müller, Chiral effective theories with a light scalar at one loop, Nucl. Phys. **B952**, 114938 (2020).

[132] O. Catà, R. J. Crewther, and L. C. Tunstall, Crawling technicolor, Phys. Rev. D **100**, 095007 (2019).

[133] T. Appelquist, J. Ingoldby, and M. Piai, Dilaton potential and lattice data, Phys. Rev. D **101**, 075025 (2020).

[134] M. Golterman, E. T. Neil, and Y. Shamir, Application of dilaton chiral perturbation theory to $N_f = 8$, SU(3) spectral data, Phys. Rev. D **102**, 034515 (2020).

[135] M. Golterman and Y. Shamir, Explorations beyond dilaton chiral perturbation theory in the eight-flavor SU(3) gauge theory, Phys. Rev. D **102**, 114507 (2020).
[136] T. Appelquist, J. Ingoldby, and M. Piai, Nearly conformal composite Higgs model, Phys. Rev. Lett. **126**, 191804 (2021).
[137] T. Appelquist, J. Ingoldby, and M. Piai, Composite two-Higgs doublet model from dilaton effective field theory, Nucl. Phys. **B983**, 115930 (2022).
[138] T. Appelquist, J. Ingoldby, and M. Piai, Dilaton effective field theory, Universe **9**, 10 (2023).
[139] Y. Aoki *et al.* (LatKMI Collaboration), Light composite scalar in eight-flavor QCD on the lattice, Phys. Rev. D **89**, 111502 (2014).
[140] T. Appelquist *et al.*, Strongly interacting dynamics and the search for new physics at the LHC, Phys. Rev. D **93**, 114514 (2016).
[141] Y. Aoki *et al.* (LatKMI Collaboration), Light flavor-singlet scalars and walking signals in $N_f = 8$ QCD on the lattice, Phys. Rev. D **96**, 014508 (2017).
[142] A. D. Gasbarro and G. T. Fleming, Examining the low energy dynamics of walking gauge theory, Proc. Sci., LATTICE2016 (**2017**) 242 [arXiv:1702.00480].
[143] T. Appelquist *et al.* (Lattice Strong Dynamics Collaboration), Nonperturbative investigations of SU(3) gauge theory with eight dynamical flavors, Phys. Rev. D **99**, 014509 (2019).
[144] T. Appelquist *et al.* (Lattice Strong Dynamics (LSD) Collaboration), Goldstone boson scattering with a light composite scalar, Phys. Rev. D **105**, 034505 (2022).
[145] A. Hasenfratz, Emergent strongly coupled ultraviolet fixed point in four dimensions with eight Kähler-Dirac fermions, Phys. Rev. D **106**, 014513 (2022).
[146] Z. Fodor, K. Holland, J. Kuti, D. Nogradi, C. Schroeder, and C. H. Wong, Can the nearly conformal sextet gauge model hide the Higgs impostor?, Phys. Lett. B **718**, 657 (2012).
[147] Z. Fodor, K. Holland, J. Kuti, S. Mondal, D. Nogradi, and C. H. Wong, Toward the minimal realization of a light composite Higgs, Proc. Sci., LATTICE2014 (**2015**) 244 [arXiv:1502.00028].
[148] Z. Fodor, K. Holland, J. Kuti, S. Mondal, D. Nogradi, and C. H. Wong, Status of a minimal composite Higgs theory, Proc. Sci., LATTICE2015 (**2016**) 219 [arXiv:1605.08750].
[149] Z. Fodor, K. Holland, J. Kuti, D. Nogradi, and C. H. Wong, The twelve-flavor β-function and dilaton tests of the sextet scalar, EPJ Web Conf. **175**, 08015 (2018).
[150] Z. Fodor, K. Holland, J. Kuti, and C. H. Wong, Tantalizing dilaton tests from a near-conformal EFT, Proc. Sci., LATTICE2018 (**2019**) 196 [arXiv:1901.06324].
[151] Z. Fodor, K. Holland, J. Kuti, and C. H. Wong, Dilaton EFT from p-regime to RMT in the ϵ-regime, Proc. Sci., LATTICE2019 (**2020**) 246 [arXiv:2002.05163].
[152] H. Cai, T. Flacke, and M. Lespinasse, A composite scalar hint from di-boson resonances?, arXiv:1512.04508.
[153] A. Belyaev, G. Cacciapaglia, H. Cai, T. Flacke, A. Parolini, and H. Serôdio, Singlets in composite Higgs models in light of the LHC 750 GeV diphoton excess, Phys. Rev. D **94**, 015004 (2016).
[154] G. Cacciapaglia, G. Ferretti, T. Flacke, and H. Serodio, Revealing timid pseudo-scalars with taus at the LHC, Eur. Phys. J. C **78**, 724 (2018).
[155] I. Brivio, M. B. Gavela, L. Merlo, K. Mimasu, J. M. No, R. del Rey, and V. Sanz, ALPs effective field theory and collider signatures, Eur. Phys. J. C **77**, 572 (2017).
[156] B. Bellazzini, A. Mariotti, D. Redigolo, F. Sala, and J. Serra, *R*-axion at colliders, Phys. Rev. Lett. **119**, 141804 (2017).
[157] M. Bauer, M. Neubert, and A. Thamm, Collider probes of axionlike particles, J. High Energy Phys. 12 (2017) 044.
[158] Y. Aoki *et al.*, Flavor-singlet spectrum in multi-flavor QCD, EPJ Web Conf. **175**, 08023 (2018).
[159] Y. Aoki *et al.* (LatKMI Collaboration), SU(3) gauge theory with four degenerate fundamental fermions on the lattice, Proc. Sci., LATTICE2015 (**2016**) 215 [arXiv:1512.00957].
[160] R. C. Brower, A. Hasenfratz, C. Rebbi, E. Weinberg, and O. Witzel, Composite Higgs model at a conformal fixed point, Phys. Rev. D **93**, 075028 (2016).
[161] Z. Fodor, K. Holland, J. Kuti, S. Mondal, D. Nogradi, and C. H. Wong, Status of a minimal composite Higgs theory, Int. J. Mod. Phys. A **32**, 1747001 (2017).
[162] T. Appelquist *et al.* (Lattice Strong Dynamics (LSD) Collaboration), Composite bosonic baryon dark matter on the lattice: SU(4) baryon spectrum and the effective Higgs interaction, Phys. Rev. D **89**, 094508 (2014).
[163] V. Drach, P. Fritzsch, A. Rago, and F. Romero-López, Singlet channel scattering in a composite Higgs model on the lattice, Eur. Phys. J. C **82**, 47 (2022).
[164] V. Drach, T. Janowski, C. Pica, and S. Prelovsek, Scattering of Goldstone Bosons and resonance production in a Composite Higgs model on the lattice, J. High Energy Phys. 04 (2021) 117.
[165] V. Drach, T. Janowski, and C. Pica, Update on SU(2) gauge theory with $N_F = 2$ fundamental flavors, EPJ Web Conf. **175**, 08020 (2018).
[166] A. Hietanen, R. Lewis, C. Pica, and F. Sannino, Fundamental composite Higgs dynamics on the lattice: SU(2) with two flavors, J. High Energy Phys. 07 (2014) 116.
[167] W. Detmold, M. McCullough, and A. Pochinsky, Dark nuclei. II. Nuclear spectroscopy in two-color QCD, Phys. Rev. D **90**, 114506 (2014).
[168] R. Lewis, C. Pica, and F. Sannino, Light asymmetric dark matter on the lattice: SU(2) technicolor with two fundamental flavors, Phys. Rev. D **85**, 014504 (2012).
[169] R. Arthur, V. Drach, M. Hansen, A. Hietanen, C. Pica, and F. Sannino, SU(2) gauge theory with two fundamental flavors: A minimal template for model building, Phys. Rev. D **94**, 094507 (2016).
[170] A. Francis, R. J. Hudspith, R. Lewis, and S. Tulin, Dark matter from strong dynamics: The minimal theory of dark baryons, J. High Energy Phys. 12 (2018) 118.
[171] V. Drach, A. Hietanen, C. Pica, J. Rantaharju, and F. Sannino, Template composite dark matter: $SU(2)$ gauge theory with 2 fundamental flavors, Proc. Sci., LATTICE2015 (**2016**) 234 [arXiv:1511.04370].
[172] T. DeGrand, Y. Liu, E. T. Neil, Y. Shamir, and B. Svetitsky, Spectroscopy of SU(4) gauge theory with two flavors of sextet fermions, Phys. Rev. D **91**, 114502 (2015).

[173] V. Ayyar, T. DeGrand, M. Golterman, D. C. Hackett, W. I. Jay, E. T. Neil, Y. Shamir, and B. Svetitsky, Spectroscopy of SU(4) composite Higgs theory with two distinct fermion representations, Phys. Rev. D **97**, 074505 (2018).

[174] V. Ayyar, T. Degrand, D. C. Hackett, W. I. Jay, E. T. Neil, Y. Shamir, and B. Svetitsky, Baryon spectrum of SU(4) composite Higgs theory with two distinct fermion representations, Phys. Rev. D **97**, 114505 (2018).

[175] G. Cossu, L. Del Debbio, M. Panero, and D. Preti, Strong dynamics with matter in multiple representations: SU(4) gauge theory with fundamental and sextet fermions, Eur. Phys. J. C **79**, 638 (2019).

[176] B. H. Wellegehausen, A. Maas, A. Wipf, and L. von Smekal, Hadron masses and baryonic scales in G_2-QCD at finite density, Phys. Rev. D **89**, 056007 (2014).

[177] T. DeGrand, Lattice tests of beyond standard model dynamics, Rev. Mod. Phys. **88**, 015001 (2016).

[178] T. DeGrand and E. T. Neil, Repurposing lattice QCD results for composite phenomenology, Phys. Rev. D **101**, 034504 (2020).

[179] V. Drach, Composite electroweak sectors on the lattice, Proc. Sci., LATTICE2019 (**2020**) 242 [arXiv:2005.01002].

[180] K. Rummukainen and K. Tuominen, Lattice computations for beyond standard model physics, Universe **8**, 188 (2022).

[181] D. B. Kaplan, Flavor at SSC energies: A new mechanism for dynamically generated fermion masses, Nucl. Phys. **B365**, 259 (1991).

[182] E. Bennett, D. K. Hong, J.-W. Lee, C. J. D. Lin, B. Lucini, M. Piai, and D. Vadacchino, Sp(4) gauge theory on the lattice: toward SU(4)/Sp(4) composite Higgs (and beyond)., J. High Energy Phys. 03 (2017) 185.

[183] J.-W. Lee, E. Bennett, D. K. Hong, C. J. D. Lin, B. Lucini, M. Piai, and D. Vadacchino, Progress in the lattice simulations of Sp($2N$) gauge theories, Proc. Sci., LATTICE2018 (**2018**) 192 [arXiv:1811.00276].

[184] E. Bennett, D. K. Hong, J.-W. Lee, C. J. D. Lin, B. Lucini, M. Piai, and D. Vadacchino, Sp(4) gauge theories on the lattice: $N_f = 2$ dynamical fundamental fermions, J. High Energy Phys. 12 (2019) 053.

[185] E. Bennett, D. K. Hong, J.-W. Lee, C.-J. D. Lin, B. Lucini, M. Mesiti, M. Piai, J. Rantaharju, and D. Vadacchino, $Sp(4)$ gauge theories on the lattice: Quenched fundamental and antisymmetric fermions, Phys. Rev. D **101**, 074516 (2020).

[186] E. Bennett, J. Holligan, D. K. Hong, J.-W. Lee, C. J. D. Lin, B. Lucini, M. Piai, and D. Vadacchino, Color dependence of tensor and scalar glueball masses in Yang-Mills theories, Phys. Rev. D **102**, 011501 (2020).

[187] E. Bennett, J. Holligan, D. K. Hong, J.-W. Lee, C. J. D. Lin, B. Lucini, M. Piai, and D. Vadacchino, Glueballs and strings in $Sp(2N)$ Yang-Mills theories, Phys. Rev. D **103**, 054509 (2021).

[188] B. Lucini, E. Bennett, J. Holligan, D. K. Hong, H. Hsiao, J.-W. Lee, C. J. D. Lin, M. Mesiti, M. Piai, and D. Vadacchino, Sp(4) gauge theories and beyond the standard model physics, EPJ Web Conf. **258**, 08003 (2022).

[189] E. Bennett, J. Holligan, D. K. Hong, H. Hsiao, J.-W. Lee, C. J. D. Lin, B. Lucini, M. Mesiti, M. Piai, and D. Vadacchino, Progress in $Sp(2N)$ lattice gauge theories, Proc. Sci., LATTICE2021 (**2022**) 308 [arXiv:2111.14544].

[190] E. Bennett, D. K. Hong, H. Hsiao, J.-W. Lee, C. J. D. Lin, B. Lucini, M. Mesiti, M. Piai, and D. Vadacchino, Lattice studies of the Sp(4) gauge theory with two fundamental and three antisymmetric Dirac fermions, Phys. Rev. D **106**, 014501 (2022).

[191] E. Bennett, D. K. Hong, J.-W. Lee, C. J. D. Lin, B. Lucini, M. Piai, and D. Vadacchino, Color dependence of the topological susceptibility in Yang-Mills theories, Phys. Lett. B **835**, 137504 (2022).

[192] E. Bennett, D. K. Hong, J.-W. Lee, C. J. D. Lin, B. Lucini, M. Piai, and D. Vadacchino, Sp(2N) Yang-Mills theories on the lattice: Scale setting and topology, Phys. Rev. D **106**, 094503 (2022).

[193] J.-W. Lee, E. Bennett, D. K. Hong, H. Hsiao, C. J. D. Lin, B. Lucini, M. Piai, and D. Vadacchino, Spectroscopy of $Sp(4)$ lattice gauge theory with $n_f = 3$ antisymmetric fermions, Proc. Sci., LATTICE2022 (**2023**) 214 [arXiv:2210.08154].

[194] H. Hsiao, E. Bennett, D. K. Hong, J.-W. Lee, C. J. D. Lin, B. Lucini, M. Piai, and D. Vadacchino, Spectroscopy of chimera baryons in a $Sp(4)$ lattice gauge theory, arXiv:2211.03955.

[195] A. Maas and F. Zierler, Strong isospin breaking in $\boldsymbol{Sp}(4)$ gauge theory, Proc. Sci., LATTICE2021 (**2022**) 130 [arXiv:2109.14377].

[196] F. Zierler and A. Maas, $Sp(4)$ SIMP dark matter on the lattice, Proc. Sci., LHCP2021 (**2021**) 162.

[197] S. Kulkarni, A. Maas, S. Mee, M. Nikolic, J. Pradler, and F. Zierler, Low-energy effective description of dark $Sp(4)$ theories, SciPost Phys. **14**, 044 (2023).

[198] E. Bennett, J. Holligan, D. K. Hong, H. Hsiao, J.-W. Lee, C. J. D. Lin, B. Lucini, M. Mesiti, M. Piai, and D. Vadacchino, $Sp(2N)$ lattice gauge theories and extensions of the standard model of particle physics, arXiv:2304.01070.

[199] K. Holland, M. Pepe, and U. J. Wiese, The deconfinement phase transition of Sp(2) and Sp(3) Yang-Mills theories in $(2+1)$-dimensions and $(3+1)$-dimensions, Nucl. Phys. **B694**, 35 (2004).

[200] V. Beylin, M. Khlopov, V. Kuksa, and N. Volchanskiy, New physics of strong interaction and dark universe, Universe **6**, 196 (2020).

[201] R. Arthur, V. Drach, A. Hietanen, C. Pica, and F. Sannino, $SU(2)$ gauge theory with two fundamental flavors: Scalar and pseudoscalar spectrum, arXiv:1607.06654.

[202] C. R. Allton *et al.* (UKQCD Collaboration), Light hadron spectroscopy with O(a) improved dynamical fermions, Phys. Rev. D **60**, 034507 (1999).

[203] C. McNeile and C. Michael (UKQCD Collaboration), The η and η' mesons in QCD, Phys. Lett. B **491**, 123 (2000); **551**, 391(E) (2003).

[204] T. Struckmann *et al.* (TXL, T(X)L Collaborations), Flavor singlet pseudoscalar masses in $N(f) = 2$ QCD, Phys. Rev. D **63**, 074503 (2001).

[205] G. S. Bali, B. Bolder, N. Eicker, T. Lippert, B. Orth, P. Ueberholz, K. Schilling, and T. Struckmann (TXL, T(X)L Collaborations), Static potentials and glueball masses from

QCD simulations with Wilson sea quarks, Phys. Rev. D **62**, 054503 (2000).

[206] V. I. Lesk *et al.* (*CP*-PACS Collaboration), Flavor singlet meson mass in the continuum limit in two flavor lattice QCD, Phys. Rev. D **67**, 074503 (2003).

[207] C. R. Allton, A. Hart, D. Hepburn, A. C. Irving, B. Joo, C. McNeile, C. Michael, and S. V. Wright (UKQCD Collaboration), Improved Wilson QCD simulations with light quark masses, Phys. Rev. D **70**, 014501 (2004).

[208] C. Urbach (European Twisted Mass Collaboration), Lattice QCD with two light Wilson quarks and maximally twisted mass, Proc. Sci., LATTICE2007 (**2007**) 022 [arXiv:0710.1517].

[209] K. Jansen, C. Michael, and C. Urbach (ETM Collaboration), The eta-prime meson from lattice QCD, Eur. Phys. J. C **58**, 261 (2008).

[210] K. Hashimoto and T. Izubuchi, eta-prime meson from two flavor dynamical domain wall fermions, Prog. Theor. Phys. **119**, 599 (2008).

[211] W. Sun, L.-C. Gui, Y. Chen, M. Gong, C. Liu, Y.-B. Liu, Z. Liu, J.-P. Ma, and J.-B. Zhang, Glueball spectrum from $N_f = 2$ lattice QCD study on anisotropic lattices, Chin. Phys. C **42**, 093103 (2018).

[212] P. Dimopoulos *et al.*, Topological susceptibility and η' meson mass from $N_f = 2$ lattice QCD at the physical point, Phys. Rev. D **99**, 034511 (2019).

[213] M. Fischer, B. Kostrzewa, M. Mai, M. Petschlies, F. Pittler, M. Ueding, C. Urbach, and M. Werner (Extended Twisted Mass, ETM Collaborations), The ρ-resonance from $N_f = 2$ lattice QCD including the physical pion mass, Phys. Lett. B **819**, 136449 (2021).

[214] X. Jiang, W. Sun, F. Chen, Y. Chen, M. Gong, Z. Liu, and R. Zhang, η-glueball mixing from $N_f = 2$ lattice QCD, arXiv:2205.12541.

[215] T. Kunihiro, S. Muroya, A. Nakamura, C. Nonaka, M. Sekiguchi, and H. Wada (SCALAR Collaboration), Scalar mesons in lattice QCD, Phys. Rev. D **70**, 034504 (2004).

[216] A. Hart, C. McNeile, C. Michael, and J. Pickavance (UKQCD Collaboration), A lattice study of the masses of singlet 0++ mesons, Phys. Rev. D **74**, 114504 (2006).

[217] S. Prelovsek, T. Draper, C. B. Lang, M. Limmer, K.-F. Liu, N. Mathur, and D. Mohler, Lattice study of light scalar tetraquarks with $\mathrm{I} = 0, 2, 1/2, 3/2$: Are σ and κ tetraquarks?, Phys. Rev. D **82**, 094507 (2010).

[218] Z. Fu, Preliminary lattice study of σ meson decay width, J. High Energy Phys. 07 (2012) 142.

[219] J. J. Dudek, R. G. Edwards, C. E. Thomas, and D. J. Wilson (Hadron Spectrum Collaboration), Resonances in coupled $\pi K - \eta K$ scattering from quantum chromodynamics, Phys. Rev. Lett. **113**, 182001 (2014).

[220] M. Wakayama, T. Kunihiro, S. Muroya, A. Nakamura, C. Nonaka, M. Sekiguchi, and H. Wada, Lattice QCD study of four-quark components of the isosinglet scalar mesons: Significance of disconnected diagrams, Phys. Rev. D **91**, 094508 (2015).

[221] R. A. Briceno, J. J. Dudek, R. G. Edwards, and D. J. Wilson, Isoscalar $\pi\pi$ scattering and the σ meson resonance from QCD, Phys. Rev. Lett. **118**, 022002 (2017).

[222] R. A. Briceno, J. J. Dudek, R. G. Edwards, and D. J. Wilson, Isoscalar $\pi\pi, K\bar{K}, \eta\eta$ scattering and the σ, f_0, f_2 mesons from QCD, Phys. Rev. D **97**, 054513 (2018).

[223] D. Guo, A. Alexandru, R. Molina, M. Mai, and M. Döring, Extraction of isoscalar $\pi\pi$ phase-shifts from lattice QCD, Phys. Rev. D **98**, 014507 (2018).

[224] A. Rodas, J. J. Dudek, and R. G. Edwards, The quark mass dependence of $\pi\pi$ scattering in isospin 0, 1 and 2 from lattice QCD, arXiv:2303.10701.

[225] F. Zierler, J.-W. Lee, A. Maas, and F. Pressler, Singlet mesons in dark $Sp(4)$ theories, in *39th International Symposium on Lattice Field Theory* (2022), arXiv:2210.11187.

[226] J.-W. Lee, B. Lucini, and M. Piai, Symmetry restoration at high-temperature in two-color and two-flavor lattice gauge theories, J. High Energy Phys. 04 (2017) 036.

[227] B. B. Brandt, A. Francis, H. B. Meyer, O. Philipsen, D. Robaina, and H. Wittig, On the strength of the $U_A(1)$ anomaly at the chiral phase transition in $N_f = 2$ QCD, J. High Energy Phys. 12 (2016) 158.

[228] K. G. Wilson, Confinement of quarks, Phys. Rev. D **10**, 2445 (1974).

[229] L. Del Debbio, A. Patella, and C. Pica, Higher representations on the lattice: Numerical simulations. SU(2) with adjoint fermions, Phys. Rev. D **81**, 094503 (2010).

[230] GitHub—claudiopica/HiRep: HiRep repository—github.com, https://github.com/claudiopica/HiRep.

[231] GitHub—sa2c/HiRep: HiRep repository—github.com, https://github.com/sa2c/HiRep.

[232] S. Duane, A. D. Kennedy, B. J. Pendleton, and D. Roweth, Hybrid Monte Carlo, Phys. Lett. B **195**, 216 (1987).

[233] M. A. Clark and A. D. Kennedy, Accelerating dynamical fermion computations using the rational hybrid Monte Carlo (RHMC) algorithm with multiple pseudofermion fields, Phys. Rev. Lett. **98**, 051601 (2007).

[234] S. Aoki, H. Fukaya, S. Hashimoto, and T. Onogi, Finite volume QCD at fixed topological charge, Phys. Rev. D **76**, 054508 (2007).

[235] G. S. Bali, S. Collins, S. Dürr, and I. Kanamori, $D_s \to \eta, \eta'$ semileptonic decay form factors with disconnected quark loop contributions, Phys. Rev. D **91**, 014503 (2015).

[236] T. Umeda, A constant contribution in meson correlators at finite temperature, Phys. Rev. D **75**, 094502 (2007).

[237] H. Neff, N. Eicker, T. Lippert, J. W. Negele, and K. Schilling, On the low fermionic eigenmode dominance in QCD on the lattice, Phys. Rev. D **64**, 114509 (2001).

[238] J. Foley, K. Jimmy Juge, A. O'Cais, M. Peardon, S. M. Ryan, and J.-I. Skullerud, Practical all-to-all propagators for lattice QCD, Comput. Phys. Commun. **172**, 145 (2005).

[239] C. Gattringer, P. Huber, and C. B. Lang (Bern-Graz-Regensburg (BGR) Collaboration), Lattice calculation of low energy constants with Ginsparg-Wilson type fermions, Phys. Rev. D **72**, 094510 (2005).

[240] R. L. Workman *et al.* (Particle Data Group Collaboration), Review of particle physics, Prog. Theor. Exp. Phys. **2022**, 083C01 (2022).

[241] G. S. Bali, V. Braun, S. Collins, A. Schäfer, and J. Simeth (RQCD Collaboration), Masses and decay constants of the η and η' mesons from lattice QCD, J. High Energy Phys. 08 (2021) 137.

[242] T. Feldmann, P. Kroll, and B. Stech, Mixing and decay constants of pseudoscalar mesons: The Sequel, Phys. Lett. B **449**, 339 (1999).

[243] T. Feldmann, P. Kroll, and B. Stech, Mixing and decay constants of pseudoscalar mesons, Phys. Rev. D **58**, 114006 (1998).

[244] T. Feldmann, Quark structure of pseudoscalar mesons, Int. J. Mod. Phys. A **15**, 159 (2000).

[245] G. Albouy *et al.*, Theory, phenomenology, and experimental avenues for dark showers: A Snowmass 2021 report, Eur. Phys. J. C **82**, 1132 (2022).

[246] A. Blondel *et al.*, Searches for long-lived particles at the future FCC-ee, Front. Phys. **10**, 967881 (2022).

[247] G. Cottin, J. C. Helo, M. Hirsch, C. Peña, C. Wang, and S. Xie, Long-lived heavy neutral leptons with a displaced shower signature at CMS, J. High Energy Phys. 02 (2023) 011.

[248] ATLAS Collaboration (ATLAS Collaboration), Search for long-lived, massive particles in events with displaced vertices and multiple jets in pp collisions at $\sqrt{s} =$ 13 TeV with the ATLAS detector, arXiv:2301.13866.

[249] M. Kaplinghat, S. Tulin, and H.-B. Yu, Dark matter halos as particle colliders: Unified solution to small-scale structure puzzles from dwarfs to clusters, Phys. Rev. Lett. **116**, 041302 (2016).

[250] R. Laha and E. Braaten, Direct detection of dark matter in universal bound states, Phys. Rev. D **89**, 103510 (2014).

[251] J. R. Andersen *et al.*, Discovering technicolor, Eur. Phys. J. Plus **126**, 81 (2011).

[252] E. Bennett, H. Hsiao, J.-W. Lee, B. Lucini, A. Maas, M. Piai, and F. Zierler, Singlets in gauge theories with fundamental matter—data release, 10.5281/zenodo.8154507.

[253] E. Bennett, H. Hsiao, J.-W. Lee, B. Lucini, A. Maas, M. Piai, and F. Zierler, Singlets in gauge theories with fundamental matter—workflow release (Zenodo, 2023), 10.5281/zenodo.8154507.

[254] J.-W. Lee, E. Bennett, D. K. Hong, H. Hsiao, C. J. D. Lin, B. Lucini, M. Piai, and D. Vadacchino, Spectroscopy of $Sp(4)$ lattice gauge theory with $n_f = 3$ antisymmetric fermions, in *39th International Symposium on Lattice Field Theory* (2022), arXiv:2210.08154.

[255] www.dirac.ac.uk.

[256] C. Bonanno, C. Bonati, and M. D'Elia, Large-N $SU(N)$ Yang-Mills theories with milder topological freezing, J. High Energy Phys. 03 (2021) 111.

[257] G. Cossu, D. Lancaster, B. Lucini, R. Pellegrini, and A. Rago, Ergodic sampling of the topological charge using the density of states, Eur. Phys. J. C **81**, 375 (2021).

[258] C. Bonanno, M. D'Elia, B. Lucini, and D. Vadacchino, Toward glueball masses of large-N SU(N) pure-gauge theories without topological freezing, Phys. Lett. B **833**, 137281 (2022).

[259] P. Jenny, A. Maas, and B. Riederer, Vector boson scattering from the lattice, Phys. Rev. D **105**, 114513 (2022).

[260] S. Gusken, U. Low, K. H. Mutter, R. Sommer, A. Patel, and K. Schilling, Non-singlet axial vector couplings of the baryon octet in lattice QCD, Phys. Lett. B **227**, 266 (1989).